EMI CHARACTERIZATION AND IMPROVEMENT OF BI-DIRECTIONAL DC/DC CONVERTERS

Dayu Qu

Thesis submitted to the Faculty of the
Virginia Polytechnic Institute and State University
In partial fulfillment of the requirements for the degree of

Master of Science
in
Electrical Engineering

Approved by

Dr. Jason Lai, Chairman

Dr. Dan Y. Chen

Dr. Alex Q. Huang

August 25th, 1999
Blacksburg, Virginia

Keywords: EMI, bi-directional DC/DC converter, electric vehicle, soft-switching, full-bridge converter, L-type converter

EMI CHARACTERIZATION AND IMPROVEMENT OF BI-DIRECTIONAL DC/DC CONVERTERS

Dayu Qu

(ABSTRACT)

A worldwide awareness of the environment is accelerating fuel cell vehicle development. With respect to power electronics, special requirement is on the development of high efficiency, high voltage ratio bi-directional DC/DC converter for fuel cell energy system management.

In this paper, two bi-directional DC/DC converters, which are developed for Ford Motor Company's fuel cell vehicle, are compared from different aspects. Comparison is concentrated on the circuit topology and EMI performance. Emphasis is placed on soft-switch, hard-switch, synchronized rectification, auxiliary start-up winding and their effect on EMI performance in this kind of isolated bi-directional converter.

Comparison includes circuits analysis and test result. The EMI test setup is described. EMI measurements are given and explained. EMI solutions for bi-directional DC/DC converter are discussed. An EMI filter is designed and final test result is given.

ACKNOWLEDGEMENTS

I want to thank my advisor, Dr. Jason Lai, for his support and guidance to my research works. Also I want to express my heartfelt thanks to Dr, Dan Chen and Dr. Alex Huang for being my committee members.

I would like to express my appreciation and thanks to Mr. Gary Florh from Ford Company for his so much help.

I want to thank all my friends in CPES for their friendship, thank those who are always there to help me and be patient to me. These individuals include Dr. Kunrong Wang, Mr. Andy Poush, Professor Wei Chen, Mr. Jindong Zhang, Mr. Kevin Motto, Mr. Yuxin Li, Mr. Dengming Peng, Mr. Jianwen Shao, and etc.

A special thanks to VPEC and CPES staff member for their excellent job and great help to my life in VPEC and CPES. They are Mr. Jeffery Baston, Ms. Teresa Shaw, Ms. Evelin Martin, Mr. Joe Price O'Brien, Ms. Trish Rose, and Mr. Steve Chen.

Finally, I want to thank and my wife and my parents for their love, support, and encouragement both in my good time and hard time.

TABLE OF CONTENTS

LIST OF FIGURES

CHAPTER I

INTRODUCTION

1.1 Background and motivation

In recent years, the activity on fuel cell research has increased rapidly. As of now several biggest automotive companies (GM, Ford, Benz, Toyota) all over the world have begun research efforts on the fuel cell development.

Fuel cells are electrochemical devices that convert fuel energy directly to electrical energy with the potential for attaining very high energy conversion efficiency. Fuel cells chemically combine the molecules of a fuel and oxidizer to generate direct current (DC) without burning, dispensing with the inefficiencies and the pollution of traditional combustion engines. The overall conversion efficiency can be approximately 85%. Air emissions from fuel cells are so low that several Air Quality Management Districts in the United States have exempted them from requiring a permit to operate.

Similar to batteries, fuel cells produce direct current (DC) power and need to be electrically connected in stacks to obtain a usable voltage. However, unlike batteries, fuel cells convert the energy from a hydrogen-rich fuel directly into electricity and operate as long as fuel and oxygen are supplied to the cell.

Fuel cells are an environmentally clean, quiet, and a highly efficient method for generating electricity from fuels. The high efficiency, quiet operation, and negligible pollutant emissions from fuel cells combine to make it a highly promising technology for automobile power applications. It may replace the existing combustion engine system to sever as the power source of vehicle in a near future. [1]

Normally a fuel cell power plant includes several parts as fuel processor, power section, and power conditioner. The power conditioner section of fuel cell consists of a converter, which converts the output voltage to a stable level to accommodate variations in load requirements.

From May, 1997, Ford Company and Oak Bridge National Laboratory begun to sponsored VPEC to develop an isolated bi-directional DC/DC converter for fuel cell management system, which will be fitted into a prototype fuel cell vehicle built by Ford Motor Company. This kind of a high frequency isolated bi-directional DC/DC converter was never designed and used before. Two prototype DC/DC converters were designed and built to demonstrate the fuel cell energy management system.

In theory, several different types of circuit topologies can be used for this converter. However, only two are selected for two prototypes. The EMI characterization of both prototypes will be discussed in this paper. And EMI solution is studied.

1.2 Fuel cell power system management

Fuel cell lack of energy storage function and it need an auxiliary power storage battery pack. In order to keep the compatibility with the today's vehicle power system, 12 V lead acid battery is preferred. The function of the battery includes: (1) boost power bus to required voltage to help start the fuel cell, and (2) store the regenerative energy from the traction motor in regenerative mode. Figure 1.1 is the conceptual block diagram of the fuel cell power management system provided by Ford motor company. [2]

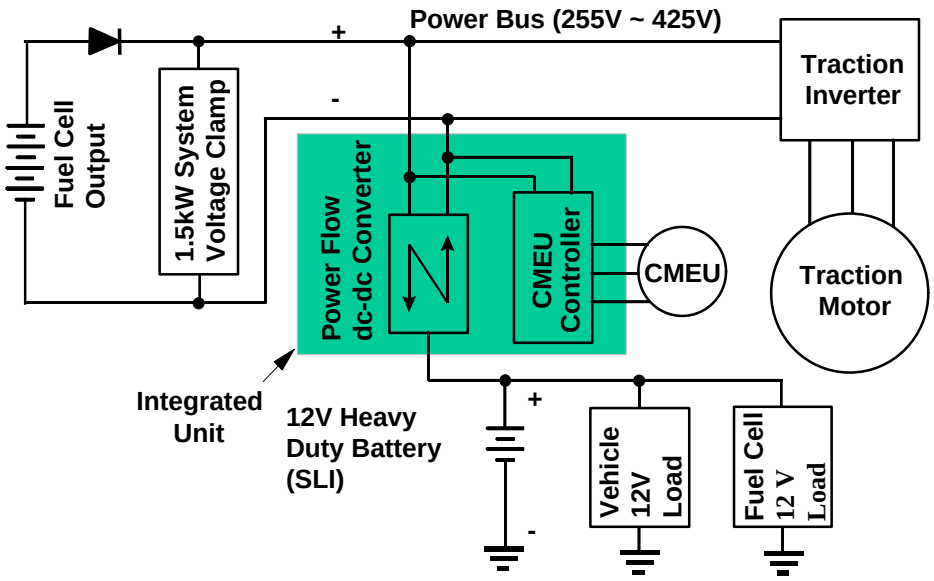

Figure 1.1 Block diagram of fuel-cell vehicle power management system

1.2.1 Operation of bi-directional DC/DC converter operation modes

There are two purposes of the bi-directional DC/DC converter. One is to boost DC power from 12 V battery to 288 V on the isolated high voltage DC bus during fuel-cell start up process. The high voltage supplied to the fuel cell compressor motor expanding unit (CEMU) controller starts up the fuel cell. After fuel cell starts up, fuel cell output feed the high voltage bus to drive the motor and at same time release the 12V battery and DC/DC converter. The power requirement for the bi-directional DC/DC converter during start up is to provide 1.6 kW DC power.

After fuel cell output voltage builds up, the bi-directional DC/DC converter should stop for about 2 seconds and switch to another operation mode automatically, which is called charging mode. In this mode, the DC/DC converter works as a battery charger and it delivers power from high voltage bus to 12 V bus to charge battery and supplies power to low voltage load. The power requirement for the charging mode is 1.6 kW.

In the vehicle breaking period, high regenerative power from the traction motor is plowed back into the high voltage bus, which needs to be consumed quickly to keep the high voltage bus voltage from exceeding 425 V to protect the fuel cell. In the regenerative mode, the battery serves as an energy storage buffer to absorb the power at maximum power rate. In this mode, the bi-directional converter delivers power as high as 5 kW from high voltage bus to 12 V bus.

It can be seen that for this fuel cell power management system, the bi-directional DC/DC converter plays an important role. For safety consideration, the bi-directional DC/DC converter also provides isolation between the two voltage buses. The design of this DC/DC converter involves not only high power but also complicate operation modes and modes transferring. All the operation modes of the converter and transfer condition are illustrated in Figure 1.2. [2]

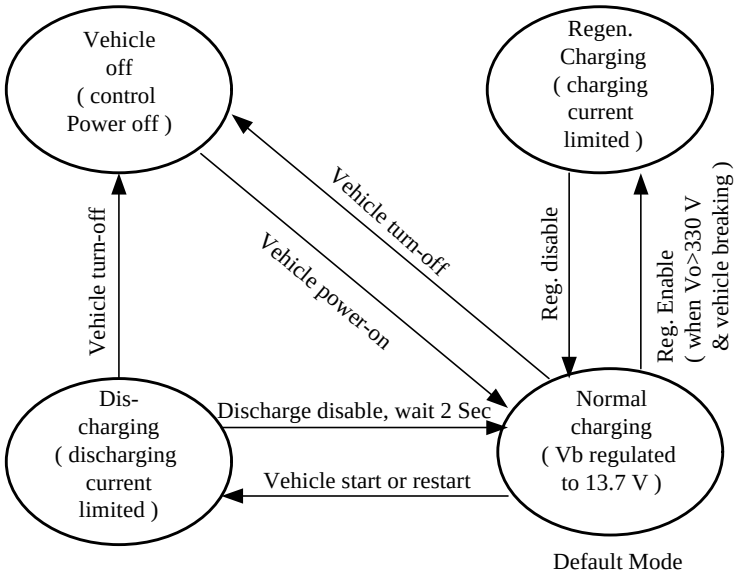

Figure 1.2 Operation modes of bi-directional DC/DC converter

1.3 System Specifications

The specifications of this bi-directional DC/DC converter for fuel cell energy management is as follows:

1. Isolated, bi-directional power flow capability, continuous power rated at 1.6 kW.
2. Heavy duty SLI (starting, lighting and ignition) battery connected to the Low voltage side. The battery voltage can swing from 8 V to 16 V.
3. In discharging mode, maximum power is 1.6 kW.
4. In normal charging mode, power is 1.6 kW.
5. In regenerative charging mode, maximum charging power is 5 kW in a maximum duration of 20 seconds. Two regenerative charging events are more than one minute apart.
6. Liquid-cooled heat sink with coolant temperature at 55°C.
7. High voltage bus capacitance is less 2000 μF.
8. More than two seconds between the end of discharging mode and beginning of charging mode.
9. Battery voltage is controlled with battery temperature compensation.
10. Start up time (the time to boost the high voltage bus higher than 255 V) is less than 200 ms when load is engaged.
11. EMI performance meets Ford Company's Component Conducted Emissions (CE) Requirements CE420, which is shown in Figure 1.3. [2][3]

Limits for Broadband Conductive Disturbances on Power Input terminals		
Frequency	Peak mode	quasi-peak mode
150 kHz—300 kHz	93 dBμV	80 dBμV
530 kHz—2 MHz	79 dBμV	66dBμV
5.9 MHz—6.2 MHz	65 dBμV	52 dBμV
30 MHz—54 MHz	65 dBμV	52dBμV
70 MHz—108 MHz	49 dBμV	36 dBμV

Figure 1.3 Conductive EMI specification for fuel cell converter

In fuel cell vehicles power management system, EMI issue is a major concern because many sensitive electronics are used in vehicle control system. Any failure of them may cause serious accidents. The EMI performance of the bi-directional DC/DC converter, which connects both high voltage power system and low voltage power system on vehicle, will affect all the power system in vehicle.

The topic of this paper is the EMI investigation and solution for the EMI problem in this kind of bi-directional DC/DC converter. The configuration of the EMI test setup is described in chapter II. Some EMI test problems only associated with the bi-directional converter is described.

In chapter III, the operating principle of both L-type and full-bridge are described. Synchronous rectification, soft-switching, and auxiliary start-up winding and their effect on the EMI are investigated. Test results are given. Multi EMI solutions are discussed. An EMI filter is designed and final spectrum measurement is given.

The conclusion is given is chapter IV. Future works are also suggested by the author.

CHAPTER II

EMI TEST SETUP AND NOISE MEASUREMENTS

In this chapter, the conductive EMI test setup and test methods are introduced. The theory of noise separation is explained. Some particular EMI testing problems, like the position of LISN and the application of EMI standard, which only exist in this kind of vehicular bi-directional DC/DC converter, are also described. EMI solutions are provided.

2.1 Conductive EMI specification for electrical vehicle application

The object of this test is to investigate the EMI performance of the bi-directional DC/DC converter in two topologies, also to study the EMI effect of the hard switch, soft switch, and synchronize rectifier technology. The test procedure will follow the CISPR 25, which is required by Ford Motor Company's Component Conducted Emissions Requirements (CE 420).

Ford Motor Company's conducted EMI standard CE 420 is formulated for traditional vehicle with combustion engine, where all the electronic equipment is connected to a 12 V bus refer to same ground. In fuel cell vehicle, the high voltage bus (traction motor drive bus) ground and the low voltage bus ground (12V bus) must be isolated for safety consideration. The two power buses are linked via the isolated bi-directional DC/DC converter. Decided by the particular connection of this converter, it could emit EMI noise to the power lines on both sides. In FCC and CISPR EMI regulations, test method for these kind of bi-directional converters is not clearly defined. Even in Ford Company's

EMC test regulation, more explanation about fuel cell vehicle power management system and bi-directional converter are still needed. Problems like, which side should the available EMI standards apply to? Should both sides have the EMI requirements, need to be answered. New EMI standards for hybrid vehicles need to be made.

2.2 Test setup

The test block diagram is shown in the figure 2.1. As required by FCC, two input power lines on high voltage side are connected through two Line Impedance Stabilization Networks (5 μH). The role of LISN here is to reject the possible conducted noise from the main power supply which may contaminate the measurements, and also to present a relatively stable impedance to the unit under test.

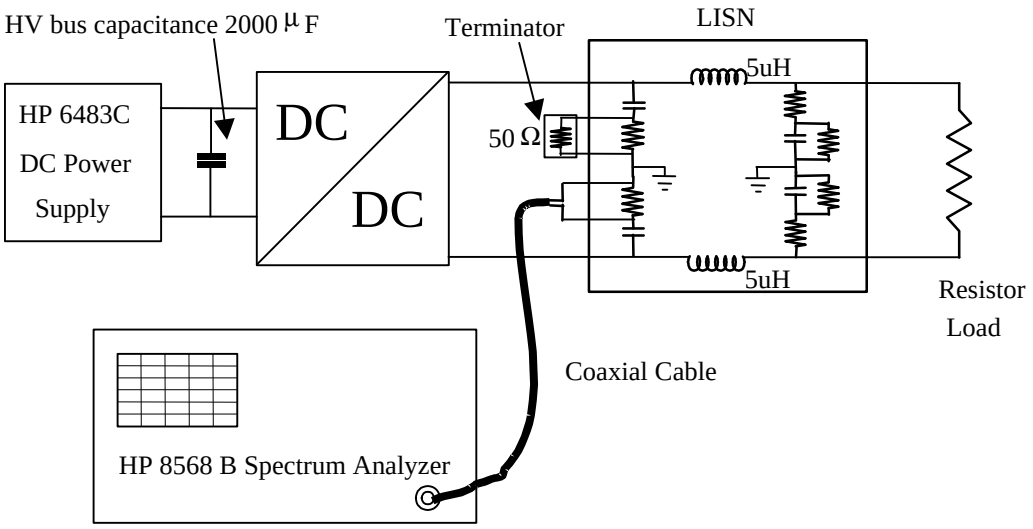

Figure 2.1 EMI test circuit

On the low voltage side, four 0.675Ω resistors connected in parallel are used as load. Two output power lines are connected through two 5 μH LISN (200 A) to the load resistors. The high current LISN (type 8616-5-TS-200-N) rates at 200 A and 5 μ. The schematic of LISN is shown in Figure 2.2. The measured impedance of LISN from load

terminal to case with 50 Ω terminator on A.F. jack is shown in figure 2.3. And the phot of the LISN is shown in Figure 2.4.

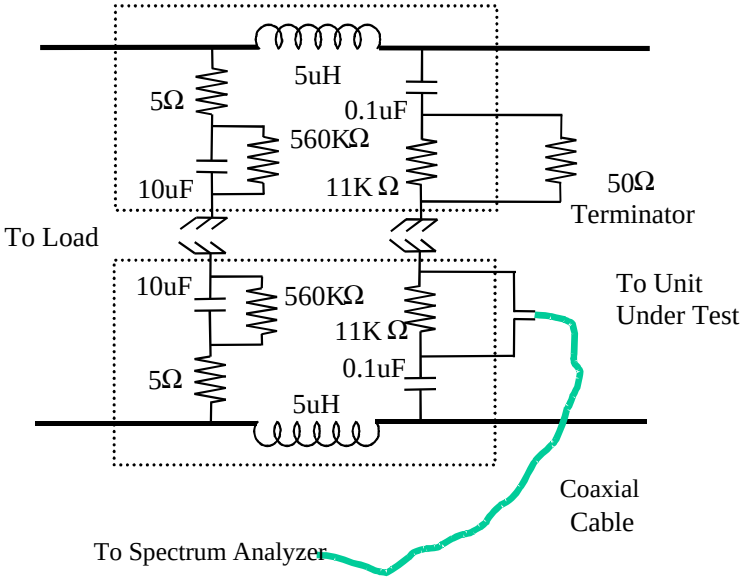

Figure 2.2 Schematic of LISN used

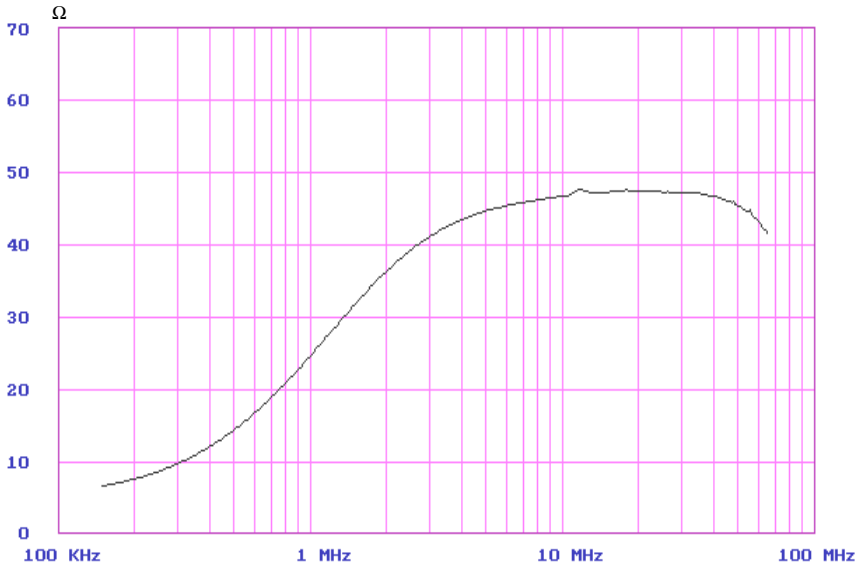

Figure 2.3 Impedance measures from load terminal to case with 50 Ω terminator on A.F. jack

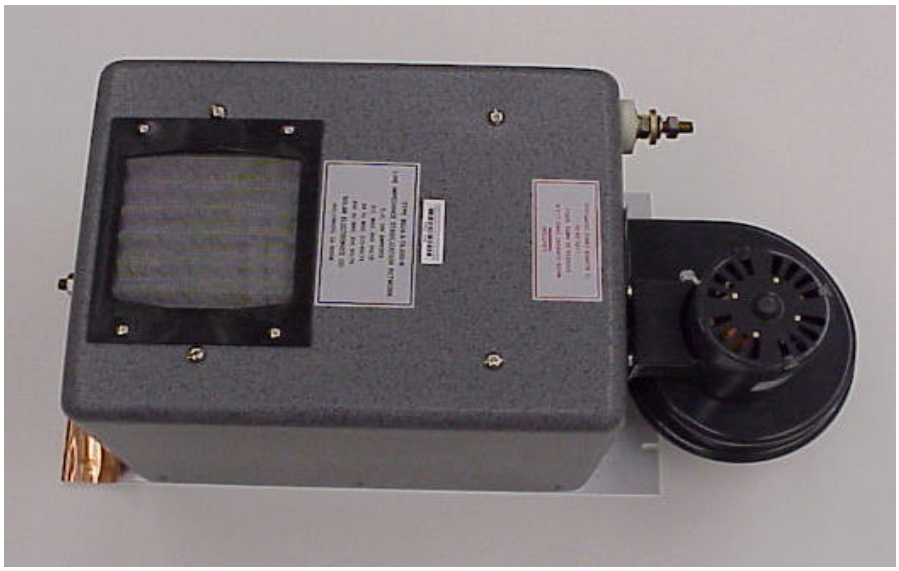

Figure 2.4 Photo of the LISN

Spectrum analyzer HP8568B is used as the noise emission receiver. Since the quasi-peak mode is not available. The spectrum analyzer is set to peak detector mode. In this way, the worst noise case will be measured. Frequency sweep range is set from 150 kHz to 108 MHz, which covers the AM and FM broadcasting frequency range. As required by Ford Motor Company's EMC regulation, resolution bandwidth is set to 10 kHz in frequency range below 30 MHz and 100 kHz in frequency range from 30 MHz to 108 MHz. So every measurement is divided into two frequency ranges, one is 150 kHz to 30 MHz while the other is 30 MHz to 108 MHz. The reference level is set to 100 dBμV with attenuation of 0 dB, an exterior 20 dB attenuator is used this test. The video bandwidth is set to be same as the resolution bandwidth in both frequency ranges.

A HP E3631A triple output linear power supply, which provides positive and negative 12 V, is used as the control circuit power supply. All driver circuits are powered by a battery with voltage of 12 V.

The surface of the test bench is covered by 2 layers of 36 mil thick sheet copper, which works as a electrical ground plane. Ground plane is connected to the electrical pipe via a 4 inch wide copper foil. Electrical pipe is connected to the ground of main utility power net. The converter, spectrum analyzer HP-8568B, and auxiliary power supply (for control circuit) are put on the ground plane. All the equipment cases, the heat sink of the converter are electrically connected to the ground plane. A HP 6843C DC power supply (600 V, 25 A) is used as the main power supply. Limited by the weight and size, the load resistor and the main power supply can not be put on the ground plane. The picture of the test bench with equipment is shown in figure 2.5. [4][5][6]

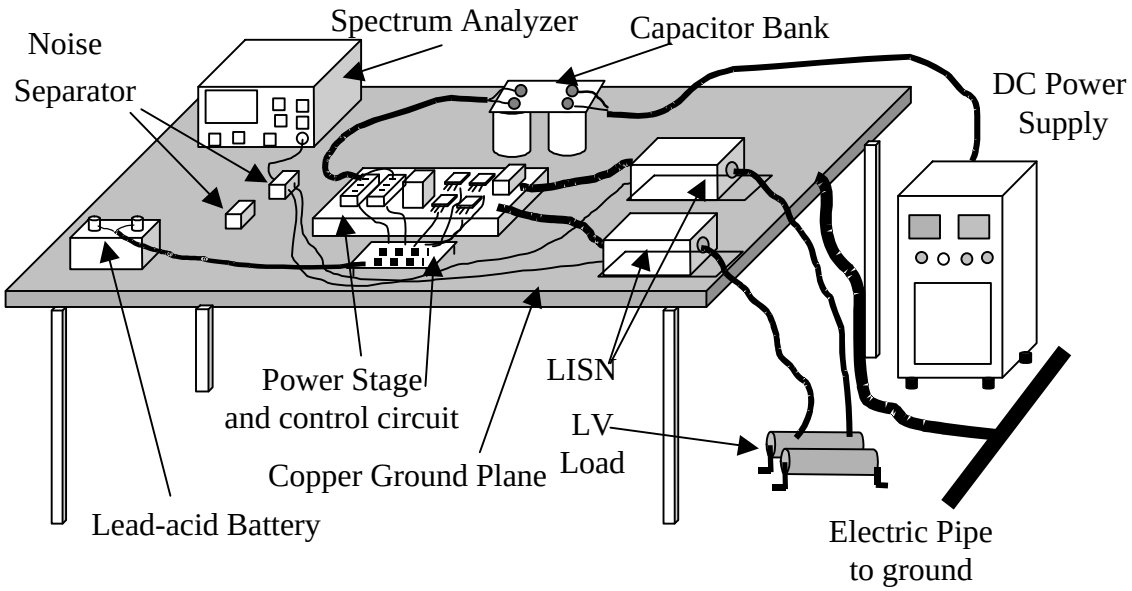

Figure 2.5 Diagram of EMI test set up

2.3 Noise measurement in the bi-directional converter

This circuit is set up to measure the total noise from low voltage sides of the bi-directional DC/DC converter.

As discussed in the first chapter, all the sensitive electronics equipment are connected to the low voltage bus. In a fuel cell driven vehicle, the converter works in boost mode only during the starting up period, which is less than 200 ms. Most of the time, this converter is working in buck mode to deliver power from high voltage bus to low voltage bus. So overall EMI performance of this converter is mostly decided by the noise generated in buck mode, and decided by the noise on the low voltage side. In this test, the noise level on the low voltage side in buck mode is selected to represent the overall EMI performance of this converter. All EMI analysis and comparison are made for measurement results from low voltage side.

2.4 EMI noise separation.

Two different kinds of noise are distinguished as Common Mode (CM) and Differential Mode (DM) noise. Though never required by FCC or CISPR, separate measurement of the Common Mode (CM) and Differential Mode (DM) noise leads to better understanding of noise source and noise propagation in a circuit. An EMI filter can then be designed to treat each mode of noise separately.

The total noise can be divided into common mode and differential mode noise by using differential mode rejection network or common mode rejection network.[7][8] In this test, two noise separators are used to measure the CM noise and DM noise independently.

CHAPTER III

OPERATION OF BI-DIRECTIONAL DC/DC CONVERTERS AND THEIR EMI CHARACTERIZATION

In this chapter, the implementation of the two prototypes DC/DC converters is described. The problems caused by hard switching and diode reverse recovery is summarized. Soft-switching implementation of the two converters is described in detail from the EMI point of view. The generation and propagation of the EMI noise in the circuit are investigated. A unique EMI problem arising from the start-up winding in isolated boost converter is reported.

3.1 Converter topology selection

High power bi-direction DC/DC converters are needed for applications like battery chargers/dischargers, UPS, hybrid vehicles, etc. In this project, a bi-directional battery charger/discharger is built. Limited by the requirements, bi-direction capability and high voltage conversion ratio dominate our consideration.

Many different circuit topologies can be used in this converter to realize bi-directional power flow capability. To help make the decision, all available circuits are narrowed down to two candidates: (1) placing voltage-fed on both sides. (2) placing current-fed on one side and voltage-fed on the other side. If voltage-fed on both side is selected, according to the specified input voltage (from 8 V to 16 V) and output voltage (from 288 V to 425 V), the turns ratio of the transformer needs to be as high as 1:45. With such a high turns ratio transformer, the voltage on the IGBT will exceed 720 V, which decides IGBT with voltage rate higher than 1000 V will be needed. And the current on low

voltage side switch will be more than 588 A Considering the manufacture problems and efficiency, the high turns ratio transformer, high current low voltage switch, and high voltage IGBT should be avoided. With current-fed on one side, it is preferred to place current fed on low voltage side. High voltage side topology is focused on voltage fed full bridge, which can be easily fabricated with IGBT modules and use the well developed phase shift technology.

Among all the current-fed topologies, L-type is the first selection because of low switch counts, low conduction loss. In a L-type converter, the transformer secondary winding carries only half of the output current. The schematic of L-type converter is shown in Figure 3.1.

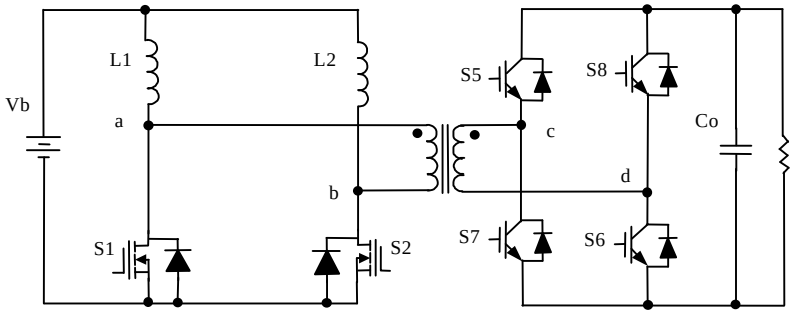

Figure 3.1 L-type converter

Another selection is current-fed full-bridge with the unified soft-switching scheme proposed in this project, which uses fewer magnetic components and achieves soft-switching easily. The Current-fed full-bridge converter is shown in Figure 3.2.

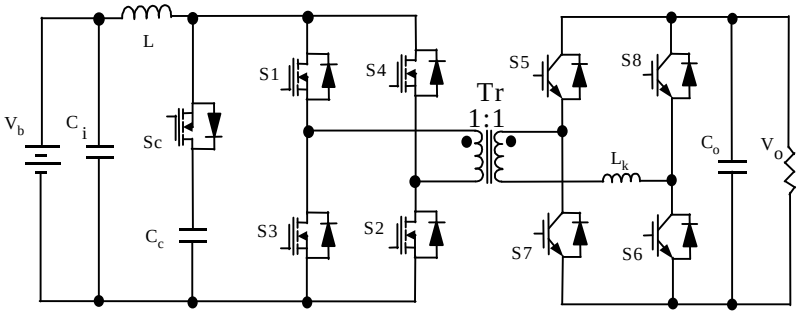

Figure 3.2 Full-bridge converter

Prototypes in both topologies were built and tested. The test result in Figure 3.3 show that the full-bridge current-fed has higher efficiency, especially in low power range.

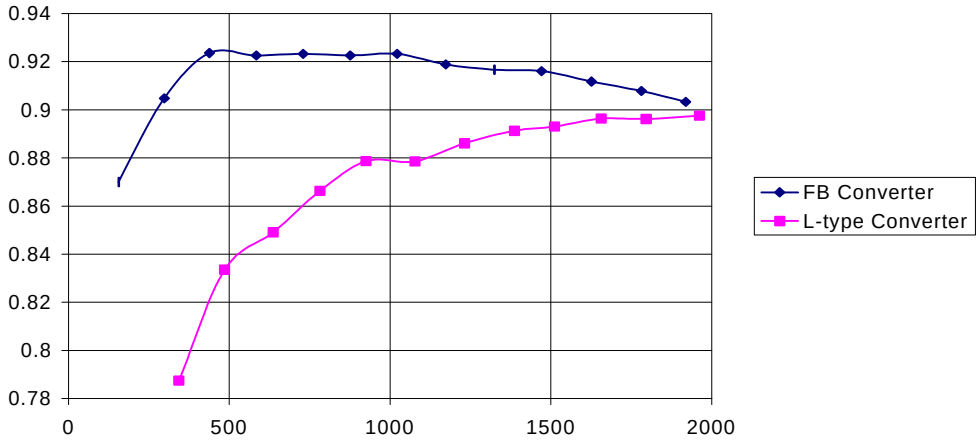

Figure 3.3 Efficiency comparison of full-bridge converter and L-type converter

Full-bridge topology is selected for its higher efficiency and soft-switching solution. But it also shows drawbacks like, expensive high quality parts are needed for the active clamp branch. Before, most of the research the has been done is about the circuit efficiency and soft switching technology. In this paper, the EMI performance of the two topologies is tested in detail. Their EMI characterization is studied. Their operation and circuit structure is studied from the EMI point of view.[9]

3.2 L-type converter

In this section, the implementation of L-type converter is described. The charging mode (buck mode) operation, which decides the EMI performance of the converter, is explained. The EMI noise measurement is given.

3.2.1 Implementation of L-type converter

L-type is selected because of its low switch counts, low conduction loss, simple transformer structure with low turns ratio and low current, and easy operation. The schematic of L-type converter is shown in figure 3.1.

This circuit is the dual of the half-bridge voltage-fed circuit topology (push-pull), but with simple transformer winding structure which conducts only half of the input current. As with any boost derived circuit topology, severe voltage ringing appears on the current-fed side switches because of the parasitic capacitance and leakage inductance in circuit. The voltage spike is so high that it will easily break down the MOSFET device. It needs to be clamped to secure the circuit operation. To solve this problem, several clamp circuits topology can be used.

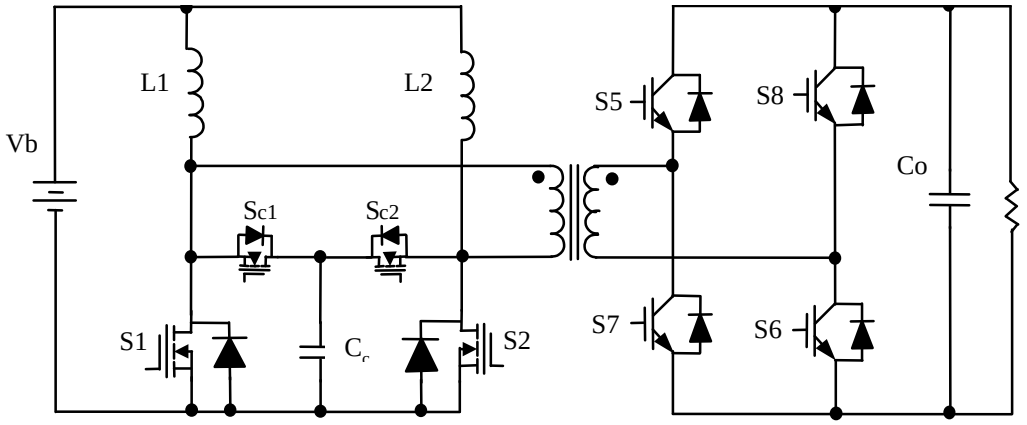

Figure 3.4 L-type converter circuit with active clamp circuit

All active clamp circuit is shown in figure 3.4. It can be used to clamp and recycle the leakage energy without power loss. So it is expected to have higher efficiency.

In this scheme, two auxiliary switches S_{c1} and S_{c2} are used to clamp the turn off voltage spike. When S_1 or S_2 is turned off, S_{c1} or S_{c2} is turned on, so the switch voltage is always clamped by the clamp capacitor C_c. The active clamp circuit needs two additional

auxiliary switches and complicated control for the auxiliary switches. The rms current rate of the auxiliary switches is not negligible. And these two auxiliary switches are working under hard switching condition and need to turn off high current pulse. That means relatively large switches are needed. Also potential EMI problem may exist.[2]

Finally, to keep the power and control circuit reasonably simple, L-type converter with RCD snubber circuit is selected for one prototype.

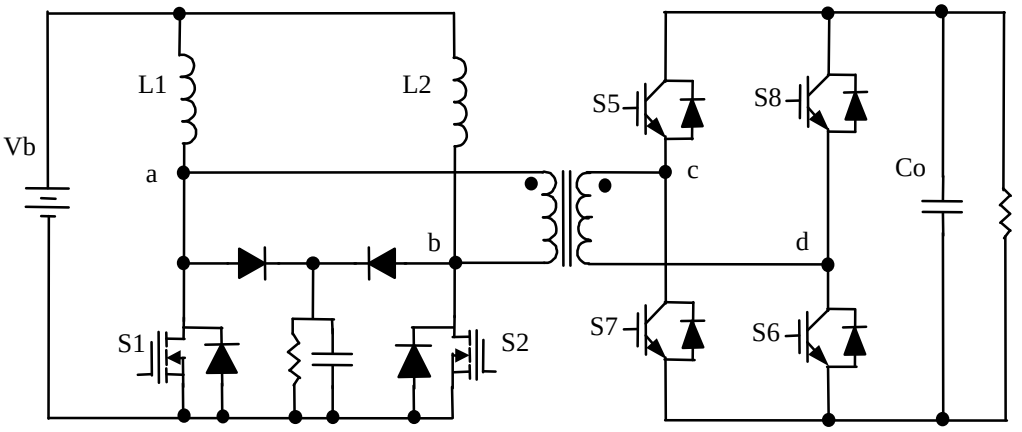

Figure 3.5 L-type circuit with RCD clamp circuit

Figure 3.5 shows the circuit schematic of the L-type prototype converter. The L-type current-fed converter is placed on the LV side, while a full-bridge voltage-fed converter is placed on the HV side. The component used are listed as following:

S_1, S_2: MOTOROLA MOSFET, MTY100N10E × 4

D_1, D_2: IR Schottky diode , 203CNQ100

S_5, S_6, S_7, S_8: MG100J2YS50, Co-packed with diode

L_1, L_2: 11 μH, Core Magnetek MC1529-1B01

Transformer, T: Core Philips E65/3F3, 3:20,

Leakage inductance Lk=25 nH @ 20 kHz measured from LV side

3.2.2 Operation of the L-type converter

The L-type bi-directional converter operates in two modes, charging and discharging mode. The mode when the battery charged by the high voltage from fuel cell is called “charging mode” or buck mode hereafter. As talked above, the EMI research work will be concentrated on the charging mode in this paper.

In the charging mode, the converter operates as a voltage-fed full-bridge converter with a current doubler output. On the HV side, the full-bridge circuit operates as an inverter with the well-known phase-shift PWM control. To reduce the diode forward voltage drop and reverse recovery time, low-voltage fast-recovery diodes other than the anti-parallel body diodes of the LV side MOSFETs are put in parallel with the MOSFETs. When no synchronous rectification is used, only the schottky diodes and MOSFET anti-parallel diodes conduct the current. With synchronous rectification, the MOSFETs are supposed to take all the current instead of the diodes.

3.2.2.1 Charging operation without synchronous rectification

Figure 3.6 shows the equivalent circuit of buck mode without synchronous rectifier.

The timing diagram and key waveforms are shown in Figure 3.7.

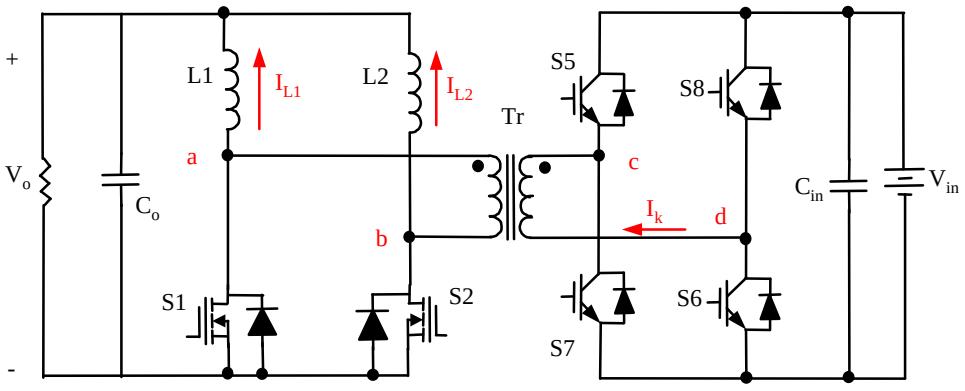

Figure 3.6 L-type converter equvalient circuit without synchronous rectifier

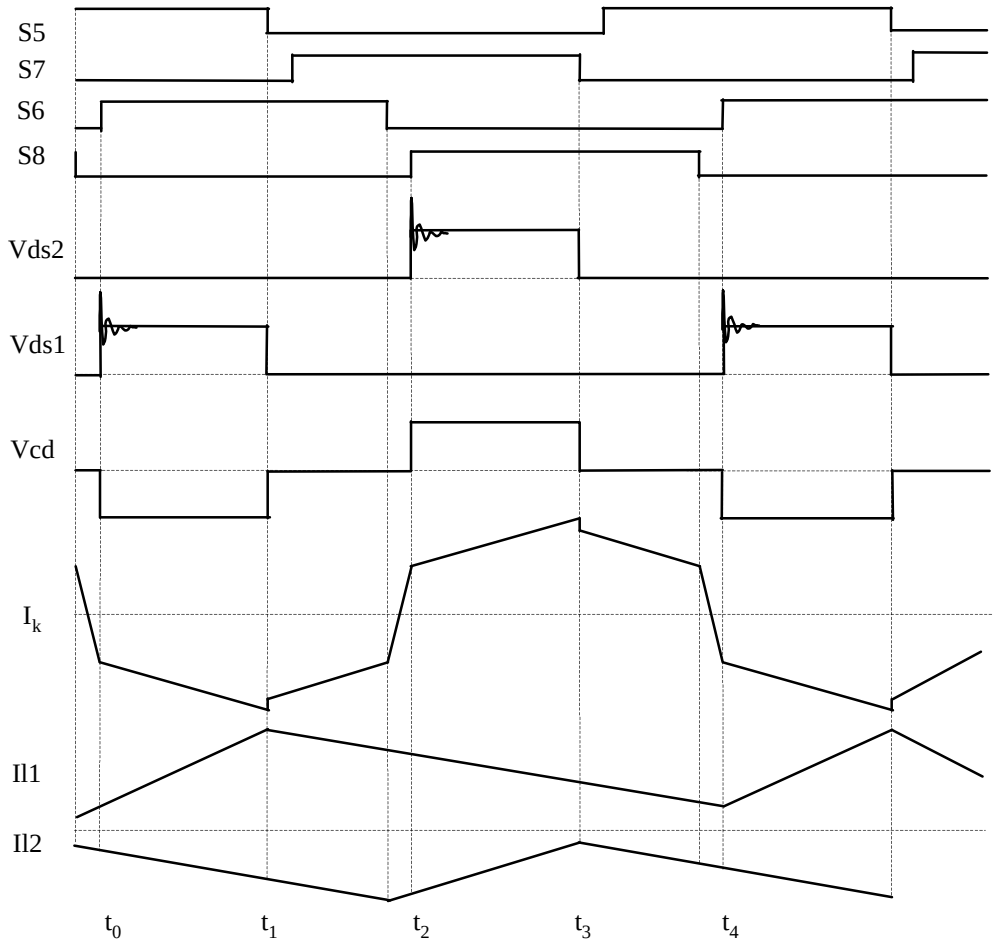

Figure 3.7 Timing diagram and key waveform of L-type converter

According to the operation of the high voltage side switch, the operation is divided into four states.

State 1 [$t_0 \rightarrow t_1$]:

Before time t_0, S_5 is already on. at time t_0, S_6 turns on and V_{ab} becomes positive at the dotted end of the secondary side. The magnetizing current starts ramping up from $-I_M$ to $+I_M$. During this state, diode D_2 is on and diode D_1 is off. Current flows in positive direction in both output inductors. The load current is supplied by the sum of currents

through L_1 and L_2. The current I_{L1} flows through D_2 and transformer secondary winding in increasing. The voltage on the inductor L_1 is V_{ab}-V_o>0. At the same time the current I_{L2} freewheeling through L_2 and D_2 is decreasing by the voltage V_o on the inductor L_2. The current through the transformer secondary winding, I_T, equals I_{L1} and accounts for half of the load current. The reflected load current also flows through S_5, the primary winding and S_6.

State 2 [$t_1 \rightarrow t_2$]:

At time t_1, S_5 turns off. S_7 will turn on. S_7 and S_6 short the primary winding at the positive supply rail. The voltage V_{ab}, on the secondary side, equals to 0V. The voltage across both inductors is $-V_o$. The conditions for L_2 do not change. Diode D_1 and D_2 are turned on by the freewheeling current I_{L1} and I_{L2}. Both inductors are in freewheeling mode.

State 3 [$t_2 \rightarrow t_3$]:

At time t_2, S_8 turns on and V_{ab} becomes negative at the dotted end of the secondary winding. During state 3, D_1 turns on and D_2 turns off. A positive voltage appears across inductor L_2 and current I_{L2} is increasing. The current through transformer secondary winding, I_T, equals inductor current I_{L2} and accounts for half of the load current.

State 4 [$t_3 \rightarrow t_4$]:

At time t_3, the full operating cycle is completed by another freewheeling period. The voltage V_T becomes zero and D_1 and D_2 are on simultaneously. $-V_o$ appears on across L_2 causing current I_{L2} to decrease while I_{L1} continues to freewheel as before. As known, the so called leading switches , S_5, S_7, which operate under ZVS turn-on. While the ZVS

turn-on of S_6 and S_8 is not secured. It is decided by the load condition and leakage inductance reflected to the high voltage side. It can be ZVS or particle ZVS.

3.2.2.2 Charging operation with synchronous rectification

The current doubler technique with synchronous rectifiers will be used to extend the soft-switching capability for the phase shift full bridge under all load conditions. Figure 3.8 introduces the power circuit and Figure 3.9 shows its basic waveforms. The operation of the HV side was already discussed before and the discussion next will be focused on the unique properties of the current doubler rectifier.

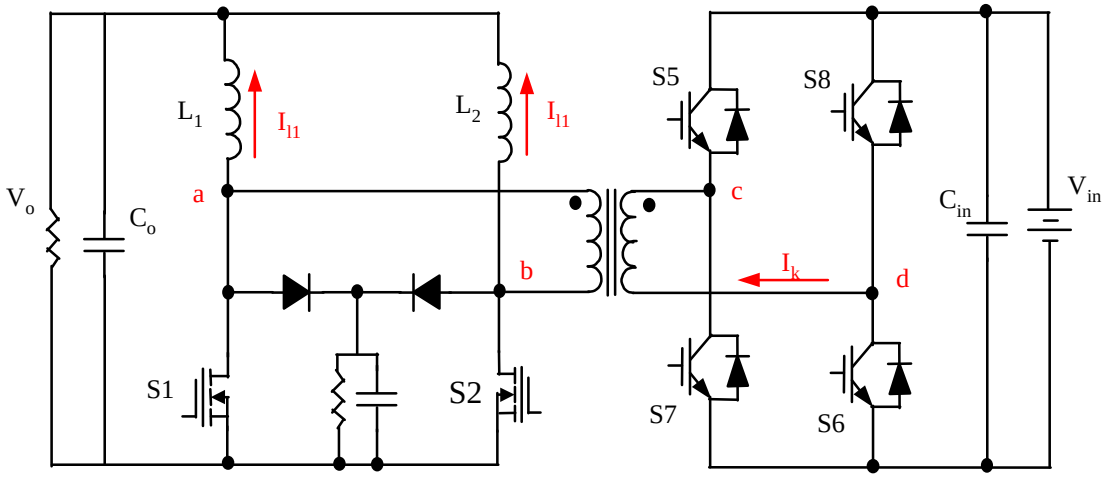

Figure 3.8 L-type converter equvalient circuit with synchronous rectifier

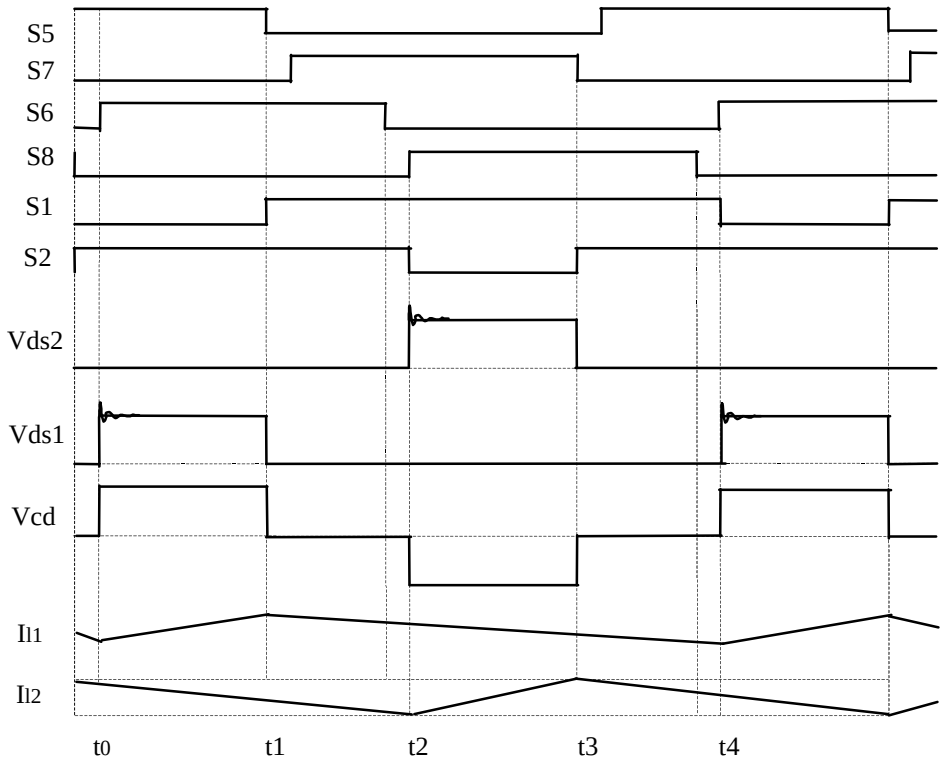

Figure 3.9 Timing diagram and waveform of synchronous rectifier

Figure 3.8 above shows the control timing and waveforms of MOSFETs synchronous operation. In accordance with the primary side, the switching period is divided in four states.

State 1 [t_0-t_1]:

At t_0, V_{ab} becomes positive. During state 1, S_1 is off and S_2 is on. Current flows in positive direction in both inductors. The sum of the I_{L1} and I_{L2} supplies the load current. The current I_{L1} flows through S_2 and the transformer secondary winding. The Voltage across L_1 is V_{ab}-V_o. This positive voltage causes the current through L_1 increase. At the same time I_{L2} freewheels through S_2 and it decreases by the rate of V_o/L_2. The current

through the secondary side of transformer equals I_{L1} and it accounts for half of the total load current.

State 2 [t_1-t_2]:

In this state, V_{ab} is zero.S_1 and S_2 are both on. The voltage across L_1 becomes $-V_o$, producing a negative slope in current I_{L1}, which now flows through S_1. The condition of L_2 do not change. Now both inductors are in freewheeling mode.

State 3 [t_2-t_3]:

At time t_3, V_{ab} becomes negative, S_1 is on and S_2 is off. A positive voltage V_{ab}-V_o appears across L_2 and I_{L2} stars decreasing. In this state, The current through the secondary side of transformer equals I_{L1}. And half of the load current flows through the transformer secondary side again. I_{L1} freewheels through S_1 and it decays by the rate of negative V_o/L_1.

State 4 [t_3-t_4]:

The full operating cycle is completed by another freewheeling period. The Voltage V_{ab} becomes zero, and S_1 and S_2 are on simultaneously. Negative V_o across both inductors causes both inductor currents to decrease.

The control timing of the current doubler rectifier can be derived from the phase-shift control signal easily.

Where $S_1=\overline{S_5}+\overline{S_6}$ and

$S_2=\overline{S_7}+\overline{S_8}$

The current doubler offers an alternative rectification method for forward, push-pull, and bridge type converters where bipolar voltage are utilized at the secondary side the isolation transformer. The synchronous rectifier operation greatly depends on the operation of the primary side switches since it has a profound effect on the current distribution during the freewheeling period. In the full-bridge converter with phase-shift control, as used in this design, currents can free flow in both primary and secondary side of the transformer windings during the freewheeling period. Thus, the current of the inductors, I_{L1} and I_{L2}, can change direction as required by the load to extend the range of the continuous conduction mode operation to lower load current values.

To avoid the body diode conducting, the synchronous switches are driven by carefully tuned timing. The turn-off of the appropriate synchronous switch must precede the switching action on the primary side. The proper timing of the MOSFET rectifiers have an important role in determining the circuit efficiency and EMI performance. Early termination of the MOSFET conduction interval will force the current into the parallel diode. Current going into the diode will make reverse recovery problem and worsen the circuit EMI performance. Conversely, delay at the turn-off of the synchronous switch will result in a shoot through situation on the secondary side of transformer

The switching speed of the synchronous MOSFET can be slowed down by increasing the series gate resistor. So, at turn-on, the schottky diode will conduct for a short time. But soon after that the MOSFET turn-on, current will go into MOSFET switch because of the lower R_{DSON} of MOSFET. In the turn-off process, slow turn-off of the MOSFET can prevent a significant portion of current flow through parallel schottkey and MOSFET body diode. In other words, the MOSFET helps to turn off current instead of all the

current being turn off by diode. As a result, parallel diode conduction and reverse recovery problem are greatly reduced, while the conduction losses won't increase a lot comparing with the no synchronous rectifier case. [9][10][11][12][13][14][15]

Improved diode reverse recovery can reduce the voltage ringing on the low voltage side. Normally this high frequency voltage ringing is thought to be a direct noise source in switching power circuit. So, with synchronous rectification, not only higher efficiency but also better EMI performance is expected.

3.3 EMI characterization of L-type

In this section, several factors which can affect EMI performance of L-type converter are discussed. The EMI spectrum measurement is given.

3.3.1 Synchronous rectification and its effect on EMI

The L-type converter was tested in buck mode for EMI characterization. And the effect of synchronous rectifier on EMI is compared with L-type hard switch operation. It is well believe that soft-switching can affect the EMI performance. In the next, effect of synchronous rectification on EMI is reported.

3.3.1.1 Time base waveform compare

When no synchronous rectification is involved, the voltage waveform on the rectifier diode is shown in figure 3. 10. Where severe voltage ringing on the diode turn off due to the diode reverse recovery can be seen, due to the diode reverse recovery problem..

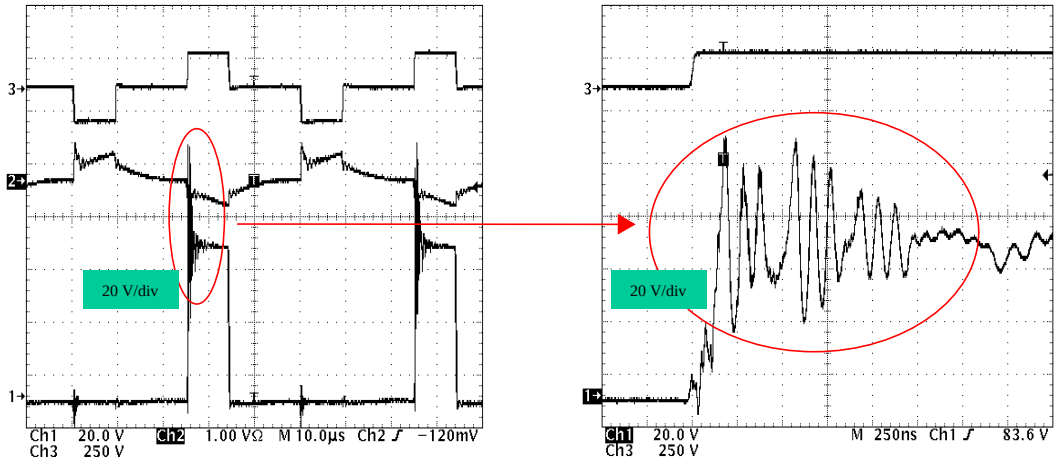

Figure3.10 Voltage waveform on rectifier diode without synchronous rectifier

The follow Figure 3.11 shows voltage waveform on MOSFET with synchronous rectification.

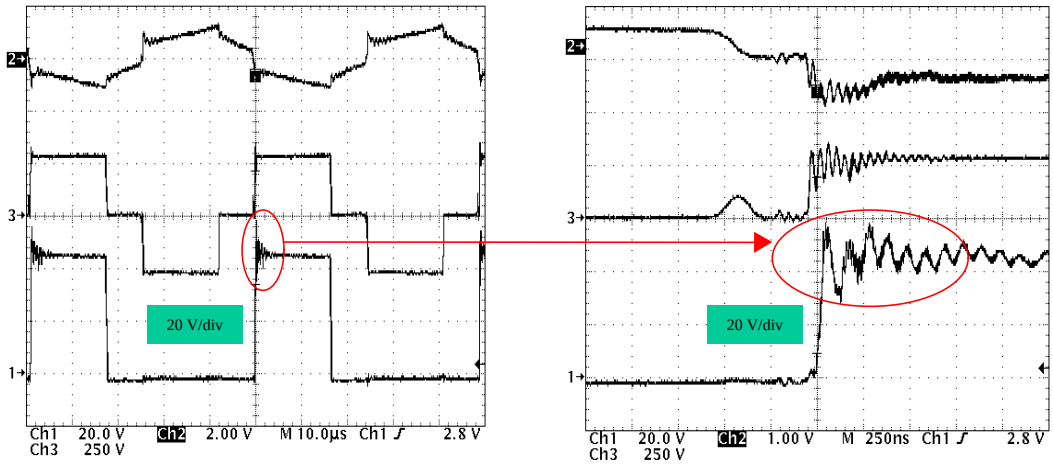

Figure 3.11 Voltage waveform on MOSFET with synchronous rectification

It can be seen from figure 3.10 and figure 3.11 that the voltage spike on the synchronous switch is reduced dramatically after synchronous rectification is used. This is because that MOSFET turns off a significant portion of current instead of the diode.

3.3.1.2 EMI spectrum comparison

This difference is also expected in the noise spectrum. The measured total noise spectrum when no synchronous rectification involved is shown in Figure 3.12.

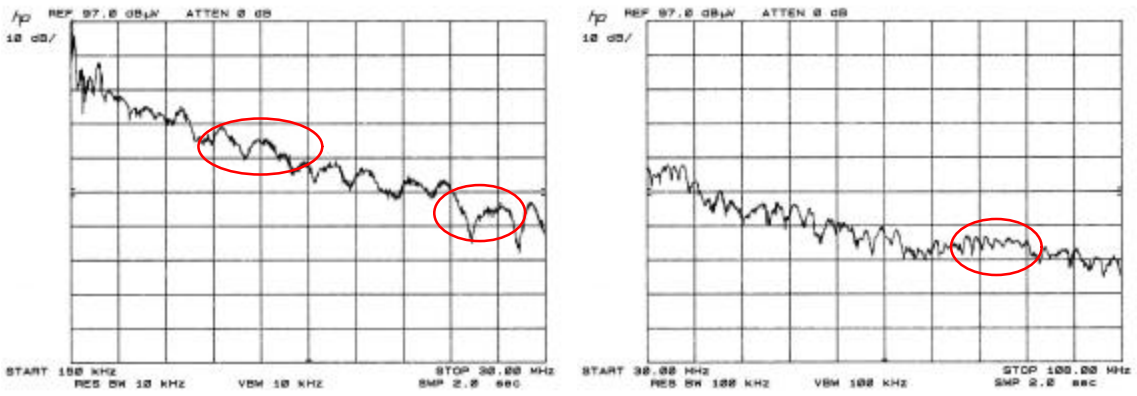

Figure 3.12 Total noise spectrum of the L-type converter without synchronous rectification

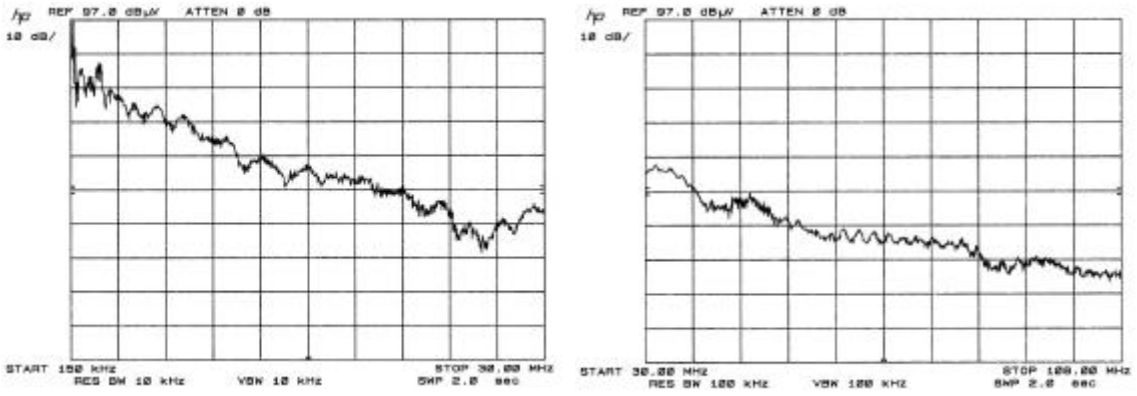

Figure 3.13 Total noise spectrum of the L-type converter with synchronous rectification

Figure 3.13 shows the total noise spectrum (150 kHz to 30 MHz, 30MHz to 108 MHz) of the L-type converter with synchronous rectifier. Figure 3.12 shows the total noise spectrum of the L-type converter under the same condition without synchronous rectifier. Both of them are under same power level, input 290 V, 3.6 A and output 12.5 V,

70 A. The spectrum results prove the analysis about the synchronous rectifier above. In the low frequency range from 150 kHz to 30 MHz, synchronous rectification help to reduce noise level at frequency 12 MHz and 25 MHz. The ringing at these frequency can be found in the time base waveform. In the high frequency range from 30 MHz to 108 MHz, no significant improvement can be found. The detail can be gotton from the CM and DM noise spectrums.

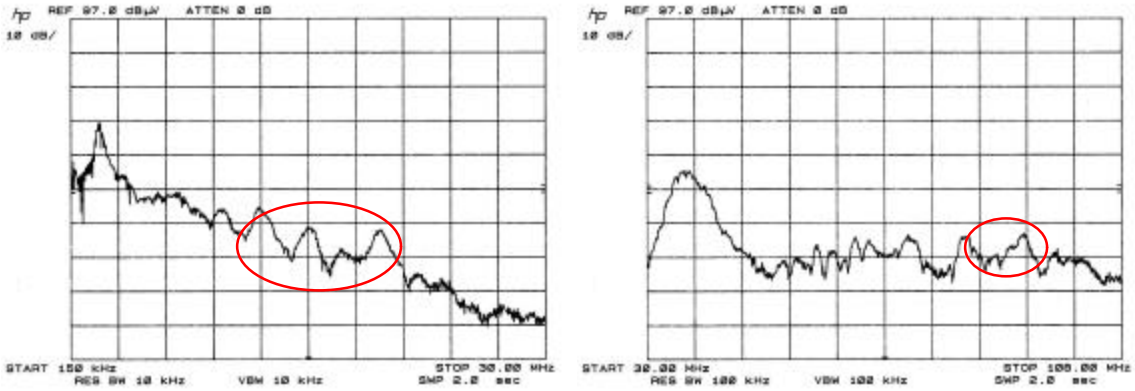

Figure 3.14 DM noise spectrum of the L-type converter without synchronous rectification

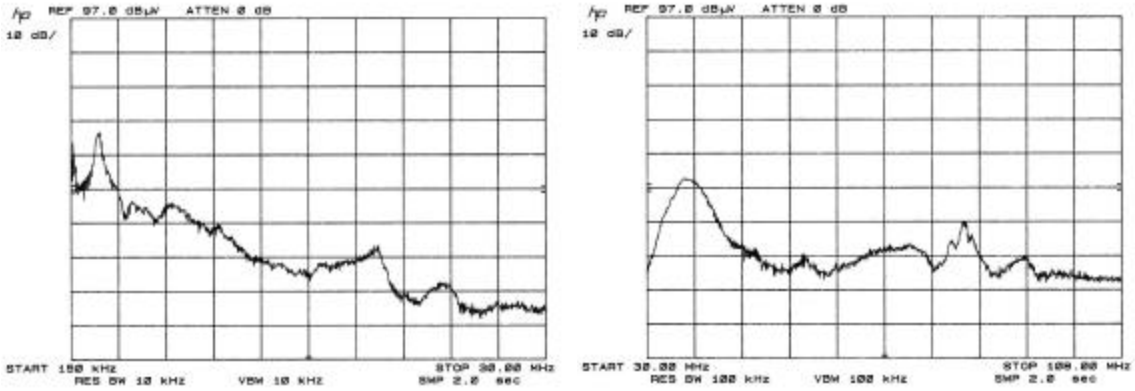

Figure 3.15 DM noise spectrum of the L-type converter with synchronous rectification

From the comparison of DM noise spectrum in Figure 3.14 and Figure 3.15, at frequency 12 MHz and 15 MHz, synchronous rectification can help reduce noise level

more than 10 dB. At the frequency of 100 MHz, synchronous rectification can reduce noise level more than 5dB. This difference is also reflected in the total noise spectrum.

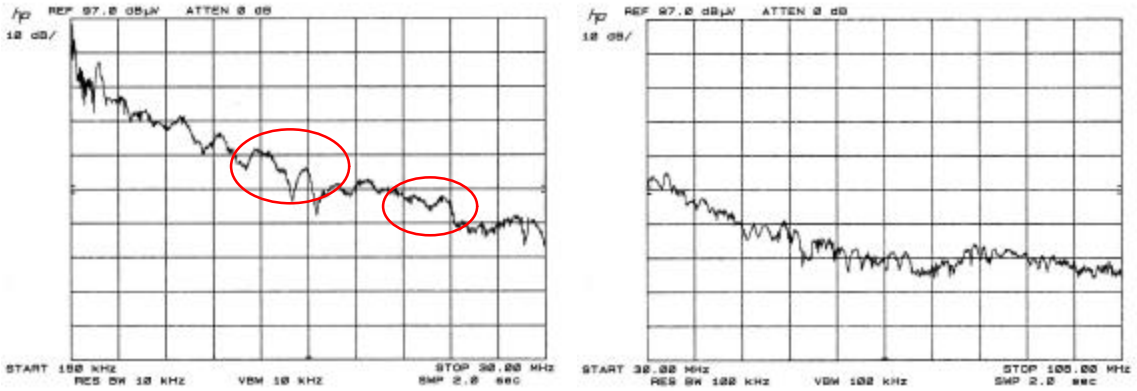

Figure 3.16 CM noise spectrum of the L-type converter without synchronous rectification

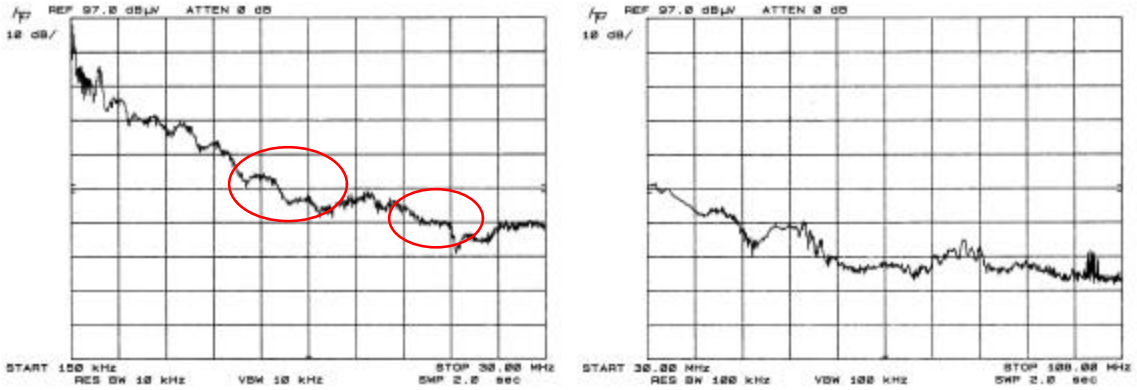

Figure 3.17 CM noise spectrum of the L-type converter with synchronous rectification

In a comparison of the CM noise level between synchronous rectifier and diode rectifier, more than 5 dB difference can be found in frequency range from 12 MHz to 15 MHz and from 23 MHz to 25 MHz. In the high frequency range from 30 MHz to 108 MHz, the improvement is not as dramatic.

3.3.1.3 Conclusion about synchronous in L-type

The comparison results of the CM nosie and DM coincide with the compoarison of total noise. They all show that synchronous recifier can improve the EMI performance by improving diode reverse recovery, which is realized by shifting the current from the diode to the MOSFET at switch turn off. In this circuit, CM noise is the main contribution to total noise. Although big improvement is found from DM noise compare, the total noise improvement is not as high as that from DM nosie.

3.3.2 Start-up winding and its effect on EMI.

3.3.2.1 Start-up winding

Like all boost derived circuit, the start-up problem needs to be dealt with when the duty cycle is less than 50%. In this circuit prototype, two start-up windings, coupling with the boost inductors, are used to help the circuit starting up. It is shown in Figure 3.18.

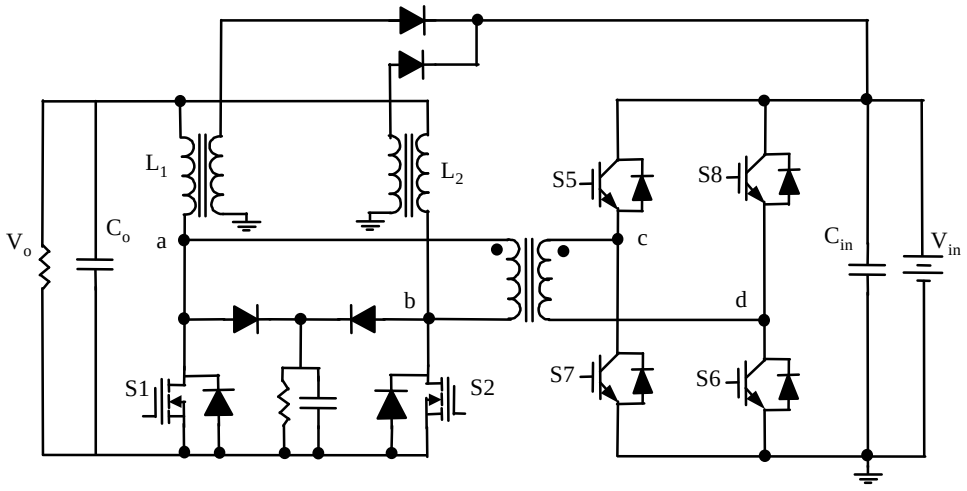

Figure 3.18 Schematic of L-type converter with start-up windings

The start-up windings are designed to work only in the start-up period. In the normal boost mode and buck mode, the rectifier diode will be reverse biased and no current goes through the start-up winding. Like all boost circuit, severe voltage ringing always happens when the switch turns off. This high frequency ringing will be coupled to the start-up winding and pass the rectifier, which can not block high frequency current. [2]

3.3.2.2 Time base waveform comparison

The current going through the start-up winding is measured in two ways, CM current and DM, which are shown in the Figure 3.19 and Figure 3.20.

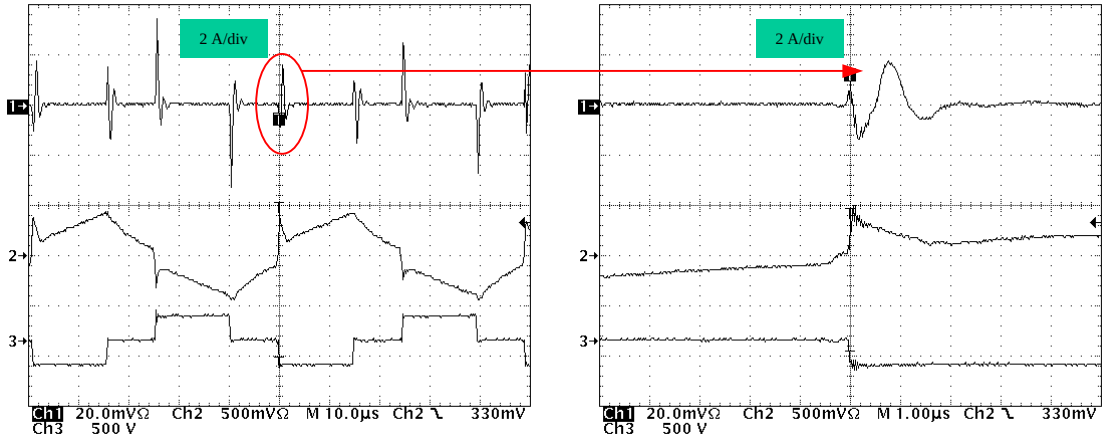

Figure 3.19 Common mode current through start-up winding

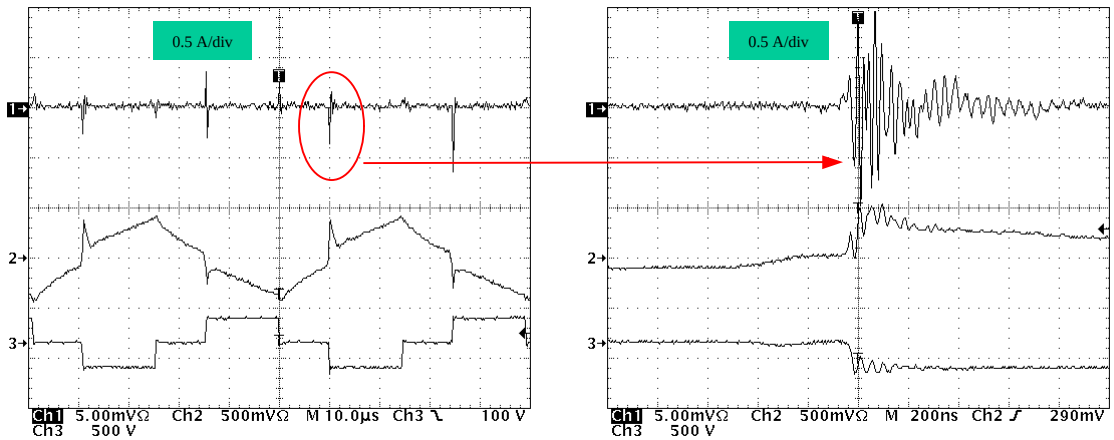

Figure 3.20 Differential mode current through start-up winding

The high frequency current ringing reflects the voltage ringing on the switches. And the high frequency components can be seen in the output current quite clearly.

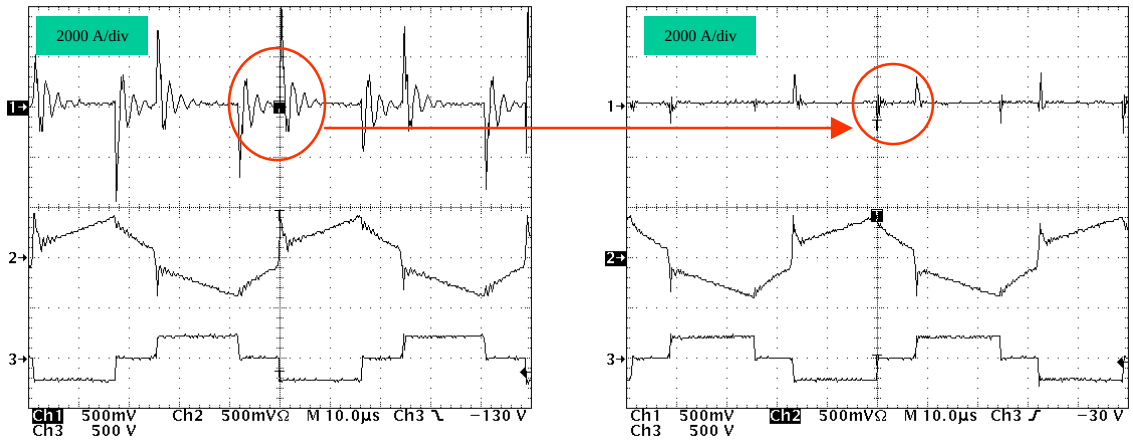

Figure 3.21 Output current when start-up winding connected (left)

and start-up winding disconnected (right)

The start-up windings link the high volatge side and the low voltage side and it become a path that one side can interfere with another side. The circulating energy which goes through the start-up winding and parasatic which exist in the flyabck winding work together and make it become a noise source. Figure 3.21 shows the output current waveforms while the circuit works under the same condition except start-up winding. It can be seen that much more current ringing will be seen on the output curent when start-up winding is connected. And this high frequency current will be seen by LISN directly. From the time base waveform, conclusion can be made that the start-up winding will be a severe noise source for both common mode and differencial mode noise. These noises will dramatica in the low frequency range and affect the EMI filter size directly.

3.3.2.3 EMI spectrum measurements comparison

The measured total noise spectrum is shown in Figure 2.22 and Figure 3.23.

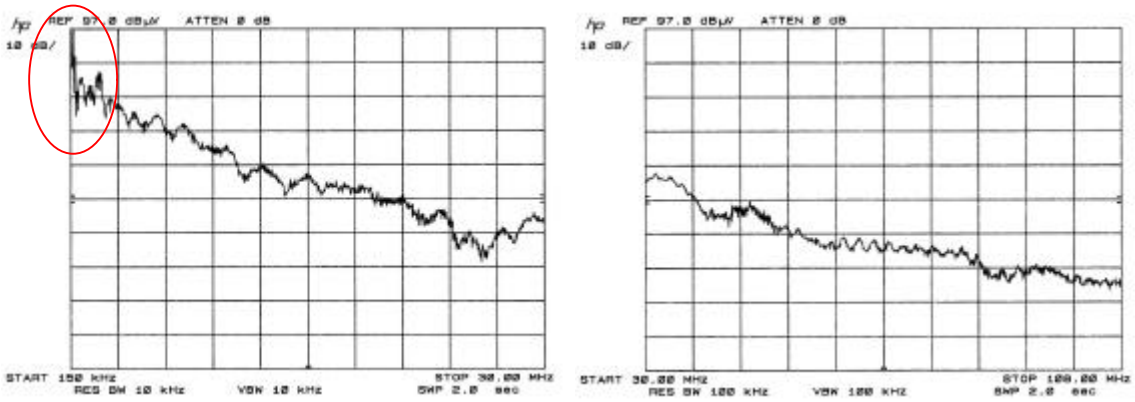

Figure 3.22 Total noise spectrum when start-up winding connected

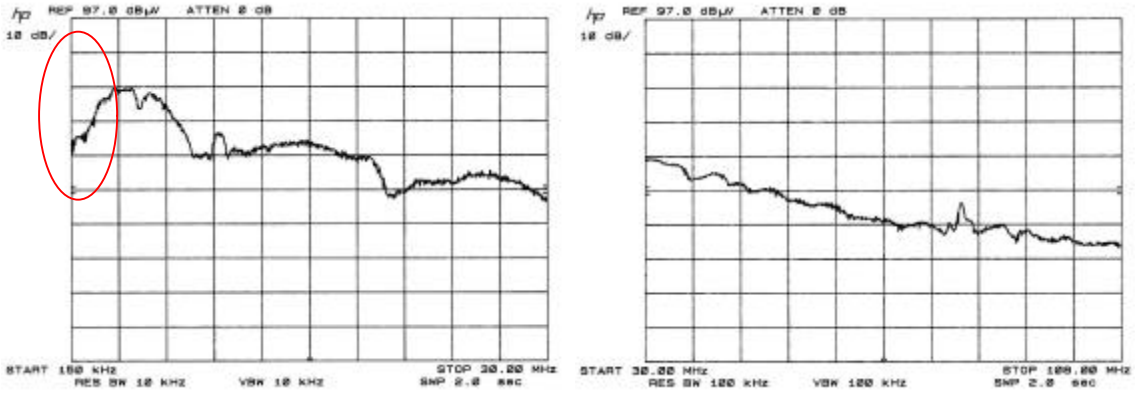

Figure 3.23 Total noise spectrum when start-up winding disconnected

Figure 3.23 shows the total noise spectrum (150 kHz to 30 MHz, 30MHz to 108 MHz) of the L-type converter when the start-up winding is disconnected from the high voltage side. Figure 3.22 shows the total noise spectrum of the full-bridge converter under same power level with start-up winding connected. It introduces a more than 30 dB higher noise level in frequency range from 150 kHz to 2.2 MHz. A big difference in the low frequency range will affect EMI filter design greatly.

Next, the effect of start-up winding on DM and CM noise is shown by CM and DM noise spectrum measurements.

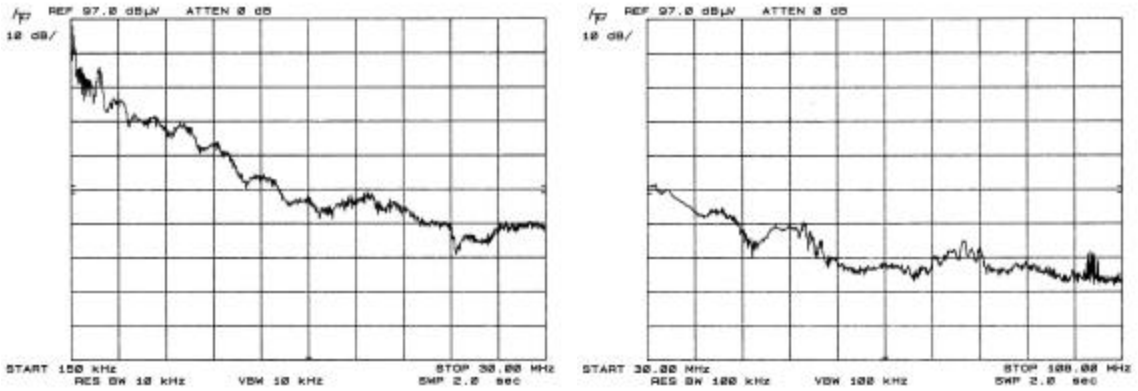

Figure 3.24 CM noise spectrum when start-up winding connected

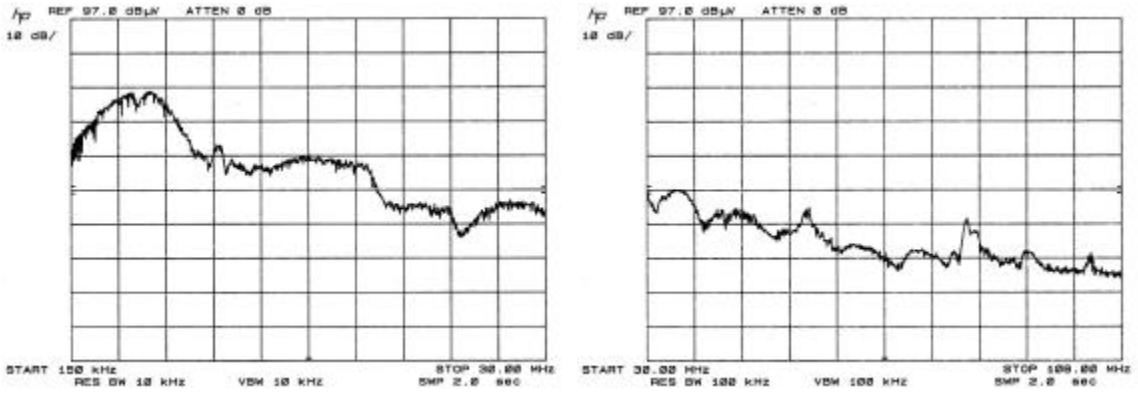

Figure 3.25 CM noise spectrum when start-up winding disconnect

Comparing common mode noise spectrum measurements in Figure 3.24 and Figure 3.25, it can be seen that the start-up winding increases CM noise level more than 30 dB in frequency 150 kHz to 2 MHz. While no obvious difference in the frequency from 30 MHz to 108 MHz.

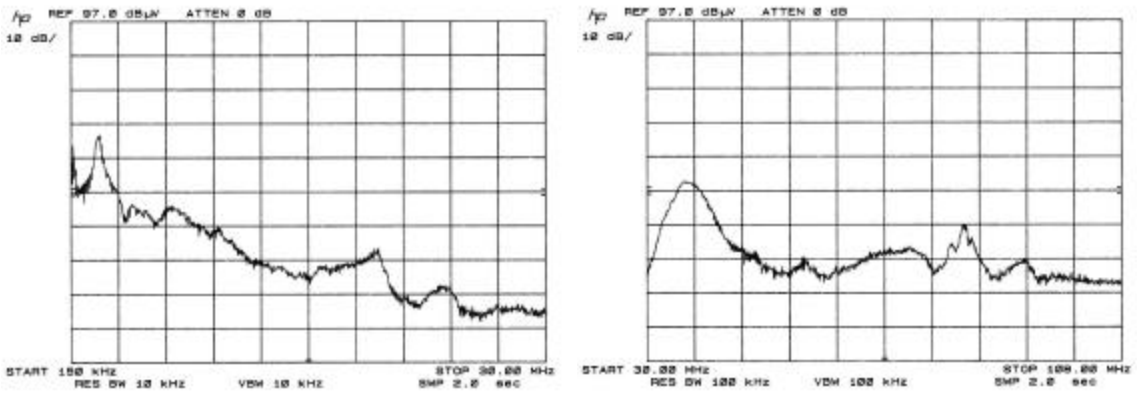

Figure 3.26 DM noise spectrum when start-up winding connect

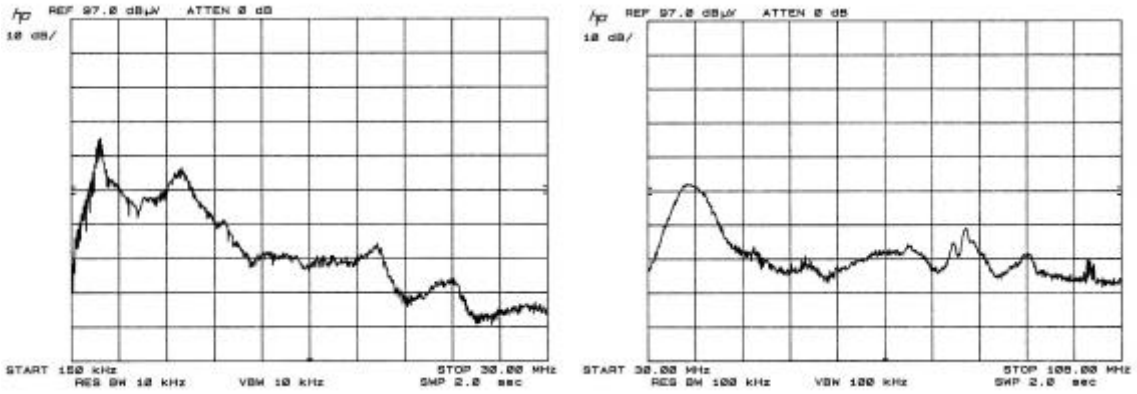

Figure 3.27 DM noise spectrum when start-up winding disconnect

From differential mode noise spectrum measurements in Figure 3.26 and Figure 3.27, it can be seen that the start-up winding increases DM noise level more than 20 dB in frequency 150 kHz to 2 MHz. While no obvious difference appears in the frequency from 30 MHz to 108 MHz.

3.3.2.4 conclusion about flyaback winding

The start-up winding in L-type converter introduces a high level of CM noise. This is because the primary side interferes with the secondary side of the isolation transformer

via start-up winding. As a result, unexpected high frequency current goes through the start-up winding. Opening the start-up winding can reduce low frequency range noise level. In real design, a mechanical relay can be used to open the start-up winding loop during buck mode.

3.4 Full-bridge converter

In this chapter, the implementation of full-bridge converter is described. The charging mode (buck mode) operation, which affects the EMI performance most, is explained. The EMI noise level is measured and results are given.

3.4.1 Implementation of full-bridge converter

The full-bridge converter topology used in this project has two active switch bridges on both sides of an isolation transformer. The bridge on high voltage side fed by a voltage source (referred to as voltage fed full-bridge) and bridge on the low voltage side fed by a current source (referred to as current-fed full-bridge). An active clamp branch placed across the current-fed bridge is used to achieve ZVZCS for the voltage-fed bridge switches in buck mode, and clamp the transient voltage on the current-fed bridge. This active clamping branch consists of an active switch and an energy storage capacitor. Synchronous rectification is used to reduce conduction loss in the current-fed bridge MOSFET switches.[9]

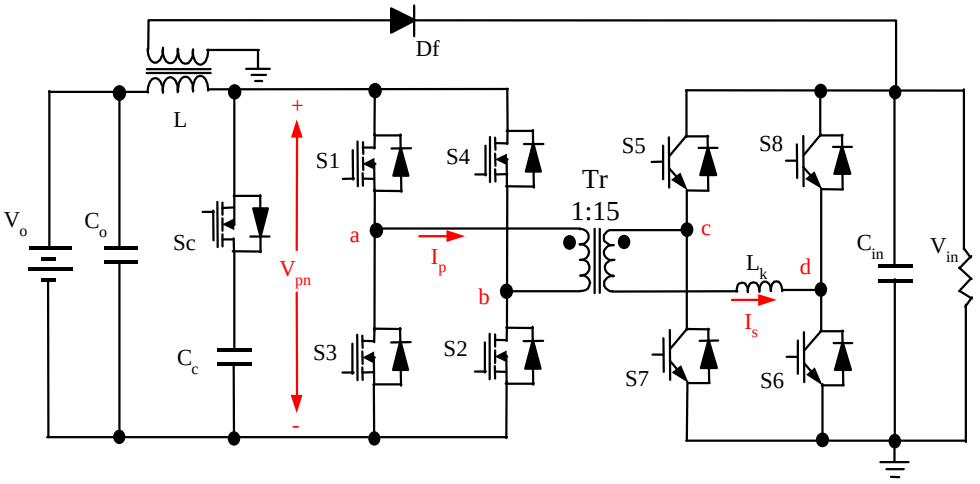

Figure 3.28 Full-bridge converter

The schematic of the full-bridge converter is shown in Figure 3.28.

The circuit is fabricated to evaluate the performance. For the primary side switches, MOSFET are selected because of the low voltage and high current rate. IGBT are selected for high side switches because of the voltage rating. The components used are listed as below:[9]

S_1, S_2, S_3, S_4:	IR 3205 55 V 100 A TO-220 Package MOSFET × 6
S_c:	IR 3205 55 V 100 A TO-220 Package MOSFET × 7
S_5, S_7	Toshiba MG100J2YS50 600 V 100 A IGBT
S_6, S_8	Toshiba MG50J2YS50 600 V 50 A IGBT
Tr:	Philips E65-3F3 core, 2:30
L:	Allied Signal AMCC-25 Metglas core, 4μH, 4 turns
C_c:	54 μF 50 V MLC capacitor × 3

3.4.2 Operations of full-bridge converter

In this section, research concentrates on the EMI performance and operation which will affect the circuit EMI performance. Charging mode is the major operation of the bi-directional DC/DC converter. In this section, charging mode operation is described. The soft switching technology and its effect on EMI is explained. The start-up winding and its effect on EMI are investigated.

3.4.2.1 Charging operation without synchronous rectification

The timing diagram and key circuit waveforms are shown in Figure 3. 29. Operation without synchronous rectification, without activation of S_1 through S_4, will be discussed first.

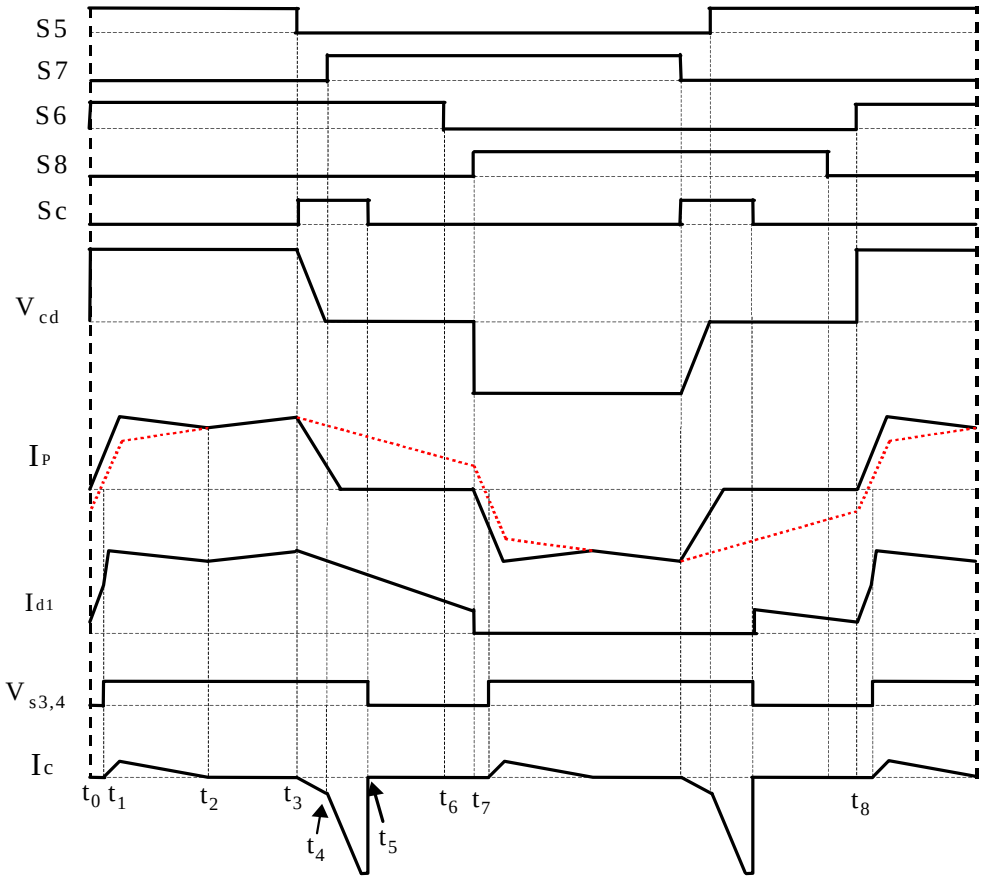

Figure 3.29 Timing diagram of charging mode with ZVZCS

Accord to the operation of the of the high voltage side bridge, the operation cycle is divided into eight states.

State 1 [t_0-t_1]:

Before time t_0, high side switch S_5 was already on, low voltage side switches are taking the freewheeling load current. At time t_0, S_6 in turned on and voltage V_{in} is applied on the high side transformer winding, and V_{cd} becomes positive. At this moment V_{cd} is only seen by the transformer leakage inductance that reflected on the high side, L_k. The current through high side transformer winding rises quickly with the slope of V_{in}/L_k. When the high side transformer current increases to the reflected load current level at t_1,

the freewheeling current will be take only by the body diodes of S_1 and S_2. Also the transformer secondary side voltage V_{ab} becomes positive and changes to reflected voltage from the high side, i.e. V_{in}/n, where n is the turns ratio. The body diodes in switch S_3 and S_4 are turned off in this moment. Diode reverse recovery problem happens at the turn-off moment, which shows up as voltage spikes on the voltage waveform.

State 2 [t_1-t_2]:

At time t_1, transformer current reaches the load current level, and V_{pn} is equal to the reflected voltage V_{in}/n. The leakage inductor L_k and the clamp capacitor C_c forms a LC resonant tank. The resonant cycle begins with the clamp capacitor charge by the current goes through the body diode of active clamp switch. This process ends at t_2 when the clamp capacitor is going to discharge but blocked by the clamp switch S_c.

State 3 [t_2-t_3]:

After time t_2, the circuit goes on to run the normal phase shift operation. The output side choke continues to be charged with the rising slope of $(V_{in}/n-V_o)/L$.

State 4 [t_3-t_4]:

At time t_3, one phase shift duty cycle ends as the turn-off of S_5, load current in the secondary side will charge the parasitic capacitance of S_5 and discharge the parasitic capacitance of S_7. Anti-parallel diode of S_7 will take the freewheeling leakage current. On the other side at the same time, S_c is turned on, and the clamp capacitor, C_c, will hold the bus voltage V_{pn} high. This voltage is reflected to the transformer secondary side, between node c and d, and applied on the leakage inductance and reset the freewheeling current.

State 5 [t_4-t_5]:

During state 5, S_7 can be turned on with ZVS because its anti-parallel diode is conducting. And freewheeling current in high voltage side continue to reduce until zero. Then anti-parallel diode of S_1 and S_2 starts to block. At the same time, the output load current is increasing is and is provided by the clamp branch.

State 6 [t_5-t_6]:

At time t_5, S_c is turned off, V_{pn} drops to zero and freewheeling cycle on the low voltage side is initiated. Output inductor freewheels through all low voltage side switches. Comparing with the normal phase shift circuit, the difference is no freewheeling current in high voltage side. As a result, the conduction loss is saved.

State 7 [t_6-t_7]:

At time t_6, S_6 is turned off under ZCS condition because the leakage current was already reset to zero.

State 8 [t_7-t_8]:

At time t_7, S_8 is turned on and the circuit begins another half cycle which is same as before. The only difference is voltage on the transformer reverses polarity and active switches change to the other diagonal pair.

In the current waveform, I_P, the dotted lines represent the current waveform under normal phase shift operation. It can be seen that high freewheeling current is reset effectively.

To summarize, the benefits of the ZVZCS talked about above include two parts. First, the conduction loss during freewheeling cycle is eliminated on the high voltage side switches. Second, turn-off loss on the high voltage side full-bridge, which is implemented

with IGBT, is reduced by shifting leakage current to the primary side. The unsecured ZVS turn-on of S_6 and S_8 is replaced by the ZCS turn-off. From EMI point, IGBT turn-off is better but MOSFET turn-off is worse. Especially the turn-off of $S_{c.}$ [9]

3.4.2.2 Charging operation with synchronous rectification

Because the low voltage side bridge switches are implemented with MOSFETs with low on resistance, synchronous rectification can be used to reduce conduction loss with little effort.

For the synchronous rectification operation, S_1 and S_2, are always simultaneously activated during the positive duty cycle ($V_{ab}>0$) while S_3 and S_4 are simultaneously activated during the negative duty cycle ($V_{ab}<0$). During the off duty cycle, all bridge switches are on to reduce conduction loss. All bridge switches need to be turned off when S_c is on. This is important to prevent shoot through of the bridge switches. The control logic expression to realize the synchronous rectification is:

$$S_1, S_2 = (S_5 + S_6)\bullet\overline{S_c}$$

$$S_3, S_4 = (S_7 + S_8)\bullet\overline{S_c}$$

In the real circuit, a dead time is need between the turn-off of S_c and turn on of S_1 through S_4, which can prevent the shoot through problem. The timing of S_1, S_2 is shown in figure 3.30. And the current through flowing through MOSFETs is also illustrated in Figure 3. 30 i.e. I_{s1}. It is assumed when MOSFET is on, all current will go through MOSFET instead of their anti-parallel diode. [9][17][18][19]

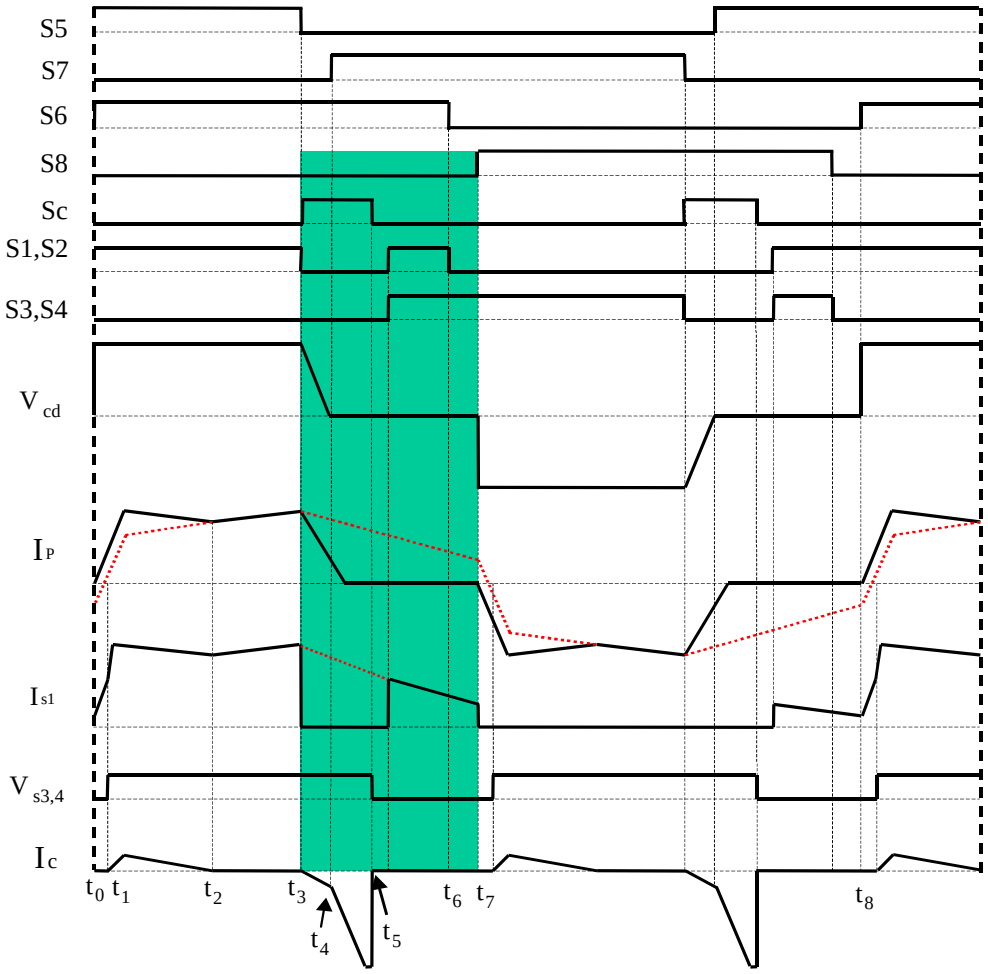

Figure 3.30 Timing diagram of charging mode with ZVZCS and synchronous rectification

3.5 EMI characterization of full-bridge converter

In this section, start-up winding, gate resistor, and soft-switching technology will be described and their effect on EMI is reported.

3.5.1 Start-up winding and its effect on EMI

Start-up winding is a necessary part for circuit to start up in boost mode. In buck mode, it is designed to be disabled in normal discharging mode and in charging mode. Its effect on EMI in charging mode is described and the measurement results are given.

3.5.1.1 start-up winding

The circuit operates as an isolated full-bridge boost converter when power is transferred from the low voltage side to high voltage side. All boost derived circuits will inevitably suffer from the high transient voltage. Another special problem with isolated boost converter is the start-up problem occurring before the output voltage is built up. The boost inductor current needs to be reset properly. The solution used in this circuit is an extra start-up winding added on the main boost inductor.

As shown in Figure 3.28, the start-up winding is connected to the high voltage side (output side in boost mode) in this circuit. The start-up winding is supposed to help circuit start up in boost mode. In buck mode, the start-up winding circuit is supposed to have no effect on circuit operation, because the rectifier diode is always reverse blocked by DC voltage in buck mode. In reality, the rectifier diode in the start-up winding circuit is invisible to high frequency current. So in buck mode, there are still high frequency currents that can go through start-up winding. The start-up winding becomes a path of unwanted high frequency current when it is not supposed to deliver power. [9]

3.5.1.2 Time base wave form measurement

In Figure 3.29, at time t_3 in state 4, when the auxiliary switch S_c turns on, clamp capacitor C_c begins to supply the load current instead of the MOSFET bridge. So high pulse current will go through the boost inductor to supply the load current. Due to the lower impedance of C_c, high frequency oscillation will generate because of the C_c and leakage inductance of the primary winding of the coupled boost inductor. The boost inductor waveform is shown in Figure 3.31.

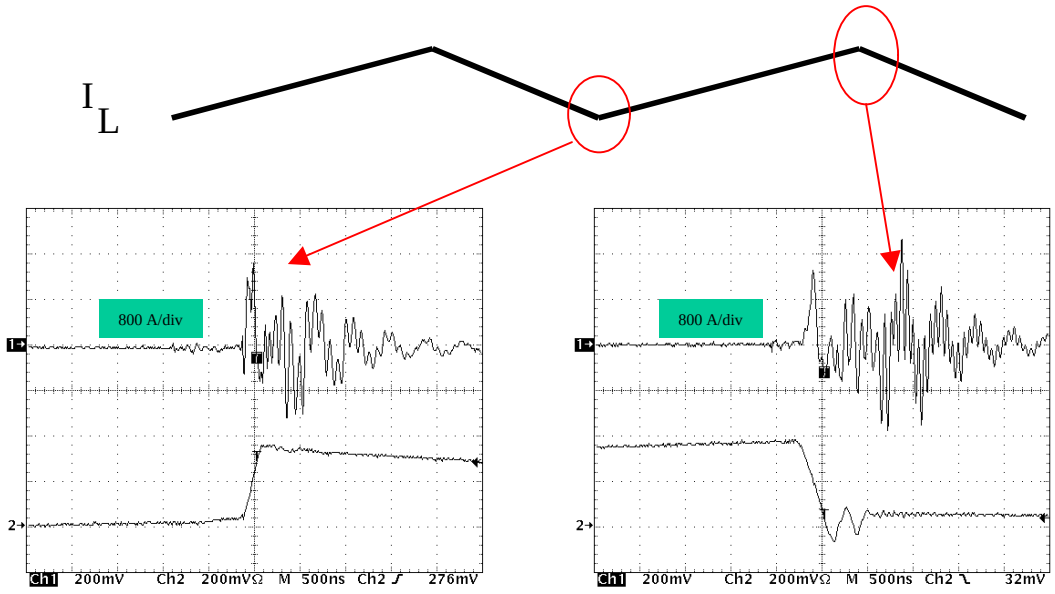

Figure 3.31 The boost inductor current when start-up winding closed

From Figure 3.31, it can be seen that the falling edge of I_L has more noise than the rising edge because of the operation of S_c and clamp capacitor. This noise current can be seen by the load and LISN.

Reflected oscillation on the secondary side of the coupled inductor will go to the high voltage side even when the fast recovery diode is reverse blocked by DC voltage. The start-up winding is actually a short for high frequency noise. The current waveform through the start-up winding secondary is shown in the Figure 3.32. The nonsymmetrical waveform shows that not only DM current but also CM current will go through the start-up winding in buck mode.

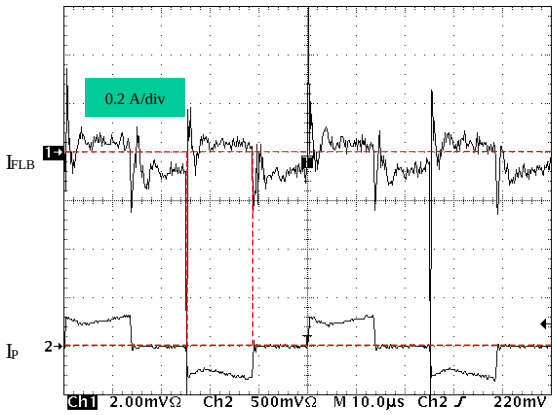

Figure 3.32 The start-up winding current waveform

The detailed CM and DM current waveforms are shown in Figure 3.33.

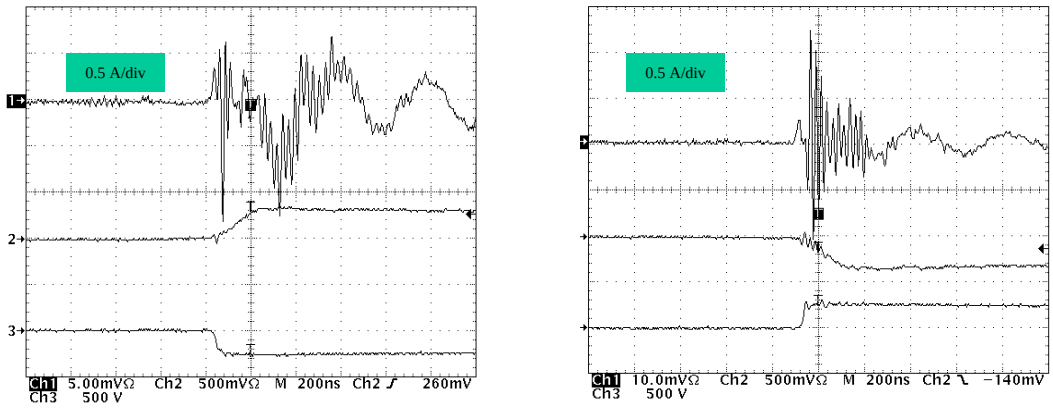

Figure 3.33 The CM current (left) and DM current (right) in start-up winding

Actually the start-up winding here is not only a noise path but also a noise source. In the switching power circuit, current or voltage waveforms on their own do not cause electromagnetic interference, whatever their spectral content. Switching of power semiconductors on their own do not cause electromagnetic interference either. The typical ideal circuit of switch mode will not cause EMI problem since the circuit parasitic is not included. Conducted EMI requires high frequency electromagnetic energy and the propagation of high frequency power in a circuit structure. A change in the switching

state of the circuit requires also the stored stray energy to change, resulting in the charge and discharge of parasitic inductance and capacitance. The value of these energies and the natural frequency of the oscillations or resistive discharge then produce the noise source. The parasitic interact with each other, creating resonance that becomes prominent noise sources.

In this circuit, the boost inductor is supposed to work as a pure inductor in buck mode. But with the secondary winding connected, high frequency noise can go through, under high di/dt condition. Also the secondary side parasitic can be reflected to the primary side, which complicates the circuit parasitic and creates a noise source. To prove this analysis, the output inductor current, I_L, is shown in Figure 3.34, when the start-up winding is open circuit. Comparing this with Figure 3.33 above, it can be seen that circuit has less oscillation when the start-up winding is disconnected.

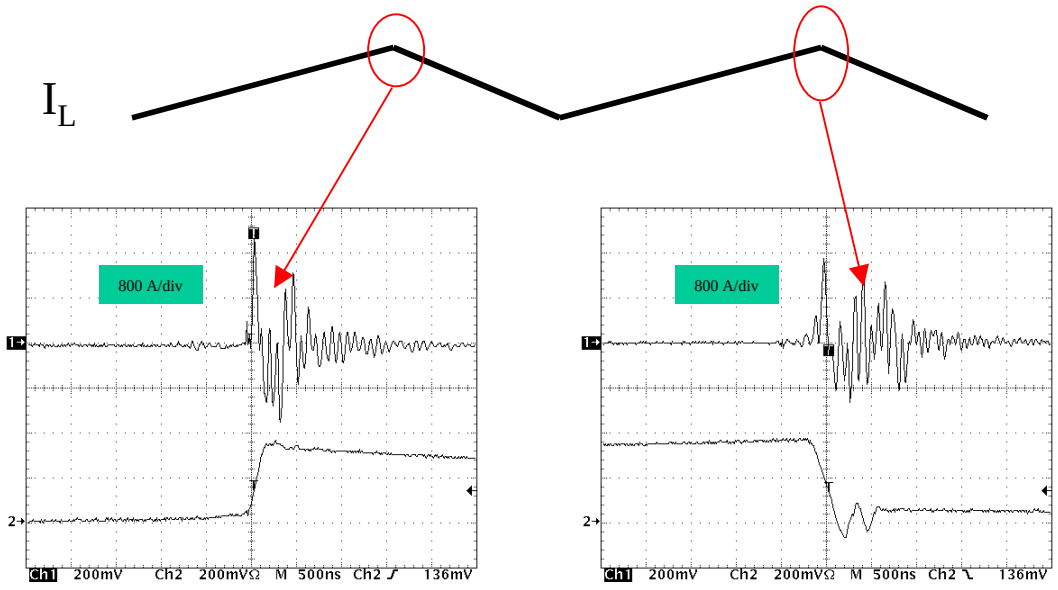

Figure 3.34 The boost inductor current when start-up winding open

3.5.1.3 EMI spectrum measurement

From the Figure 3.34, when the start-up winding is open, boost inductor is more like a pure inductor without any affect from start-up winding. Reduced parasitics results in reduced oscillation current.

The boost inductor is series connected on the low voltage side. Any high frequency components in the inductor current will appear on LISN. Even with the start-up winding disconnected, the oscillation at falling edge is still worse than rising edge because the operation of the Sc and C_c. Next, the noise spectrums are measured to prove the analysis above.

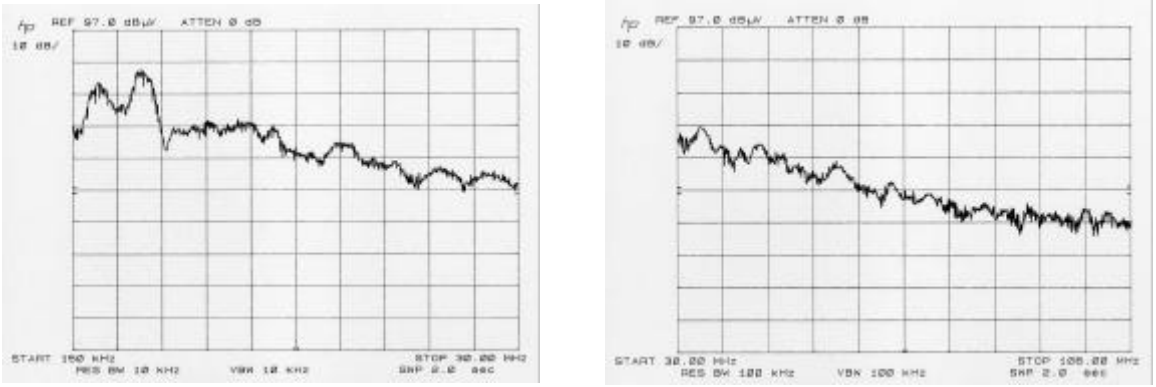

Figure 3.35 Total noise spectrum with start-up winding disconnected.

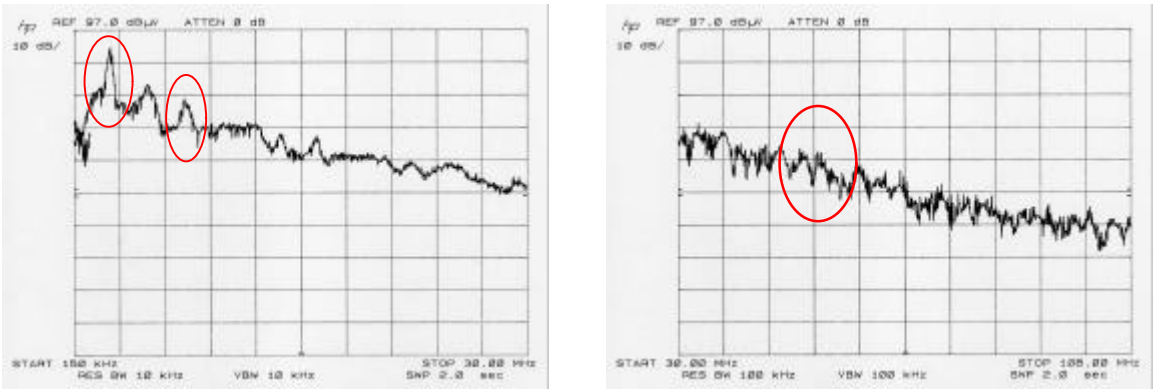

Figure 3.36 Total noise spectrum with start-up winding connected.

Figure 3.5 shows the total noise spectrum (150 kHz to 30 MHz, 30MHz to 108 MHz) of the full-bridge converter when the start-up winding is disconnected from the high voltage side. Figure 3.36 shows the total noise spectrum of the full-bridge converter under same condition with start-up winding is connected. Both of them are under same power level. The spectrum results prove the effect of the start-up winding. It introduces big parasitic and increases the total noise level by more than 10 dB at frequencies 2.6 MHz and 7.5 MHz, also it increases the noise level more than 5 dB in the frequency range from 30 MHz to 108 MHz.

The detail of the noise compare is shown in the DM and CM noise spectrums.

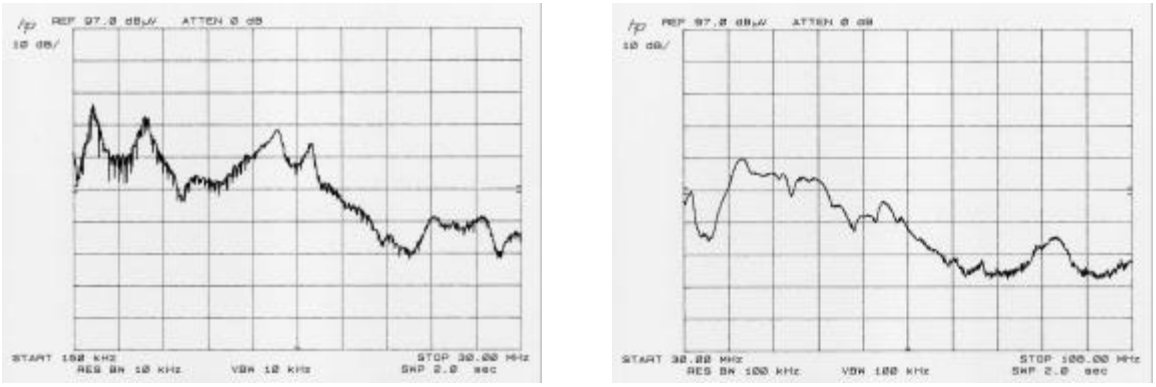

Figure 3.37 DM noise spectrum with start-up winding disconnected.

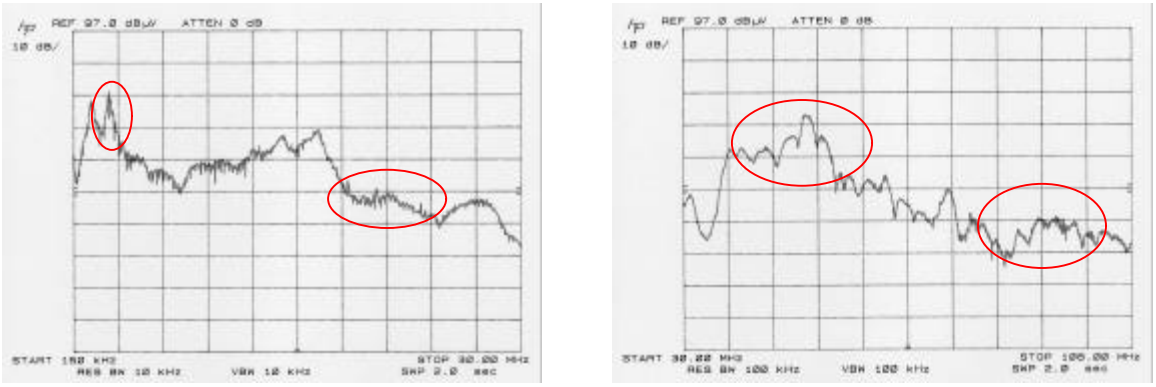

Figure 3.38 DM noise spectrum with start-up winding connected.

The DM noise spectrum comparison shows that the start-up winding can increase the DM noise level by more than 10 dB at 2.6 MHz and 20 MHz. In the high frequency range from 30 MHz to 108 MHz, it increases DM noise level dramatically, especially at 50 MHz and 77 MHz, the difference can be as high as 20 dB. In fact, the time based inductor current waveform in Figure 3.33 and start-up winding current waveform in Figure 3.32 show this difference already. The 50 MHz noise components and the 2.5 MHz noise components can be found both in the start-up winding current and the boost inductor current when the start-up winding is connected. When the start-up winding is disconnected, the 50 MHz noise components and 2.5 MHz noise components are reduced a lot in the inductor current waveform as shown in Figure 3.38

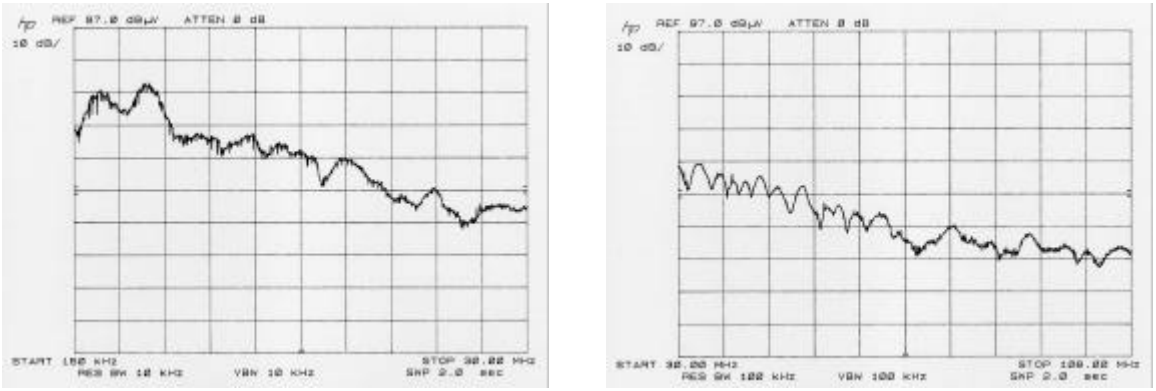

Figure 3.39 CM noise spectrum with start-up winding disconnected.

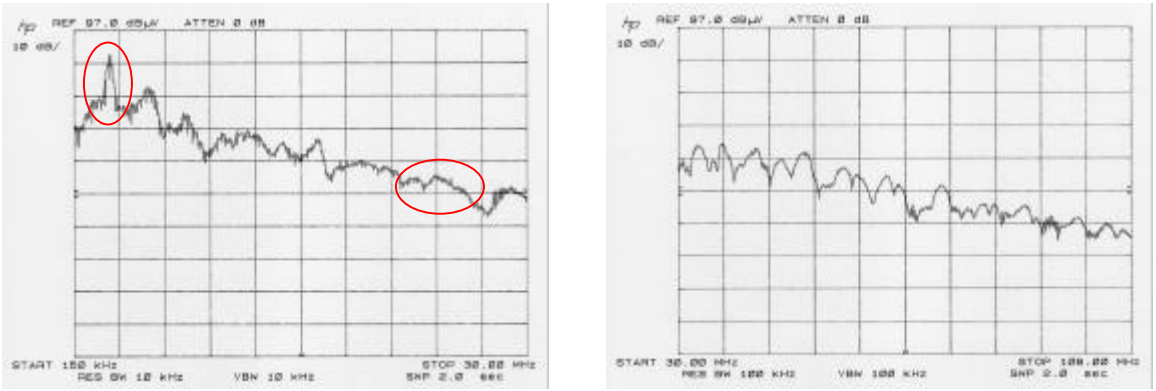

Figure 3.40 CM noise spectrum with start-up winding connected.

The CM noise spectrum comparison shows that the start-up winding can increase the CM noise level more than 10 dB at 2.6 MHz and 20 MHz-27 MHz. In the high frequency range from 30 MHz to 108 MHz, it increases CM noise level dramatically. This difference also can be found by comparing the time base inductor current waveform in Figure 3.33 and start-up winding current waveform in Figure 3.34.

3.5.1.4 Conclusion about the start-up winding in full-bridge converter

As in the L-type converter, the start-up winding in full-bridge converter also plays the role of EMI noise source and path. The EMI noise caused by start-up winding is quite significant. It can be gotten rid of with little effort. The noise from flyback is mainly in the low frequency range. Reducing the noise level in low frequency range is important for EMI filter design.

3.5.2 Active Clamp in full-bridge circuit and its effect on EMI

In the charging mode, the active clamp switch, S_c, is only activated briefly after the execution of an active duty-ratio to reset the transformer leakage current which otherwise will circulates in the voltage-fed side bridge during the off duty-cycle. Due to the operation of active clamp circuit, the so called lagging leg switches, S_6 and S_8, can realize zero-current-switching (ZCS). The great benefit of S_c here is resetting freewheeling current to save conduction loss, and make the switch S_6 and S_8 change from ZVS to ZCS to be independent from load condition.

From the EMI point of view, the activation of S_c may not improve the EMI performance a lot by just change S_6 and S_8 from ZVS turn on to ZCS turn off. Detail EMI test results are shown in Figure 3.41 and Figure 3.42.

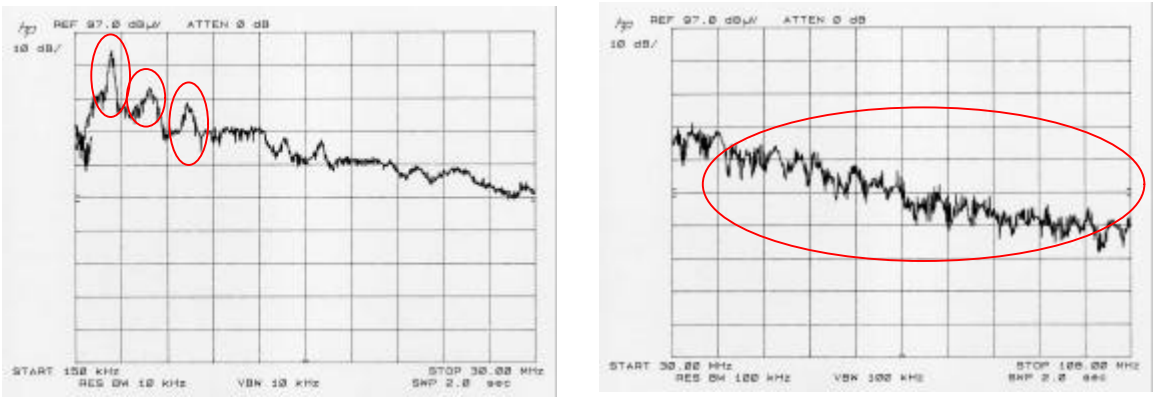

Figure 3.41 Total noise spectrum of full-bridge converter with active clamp

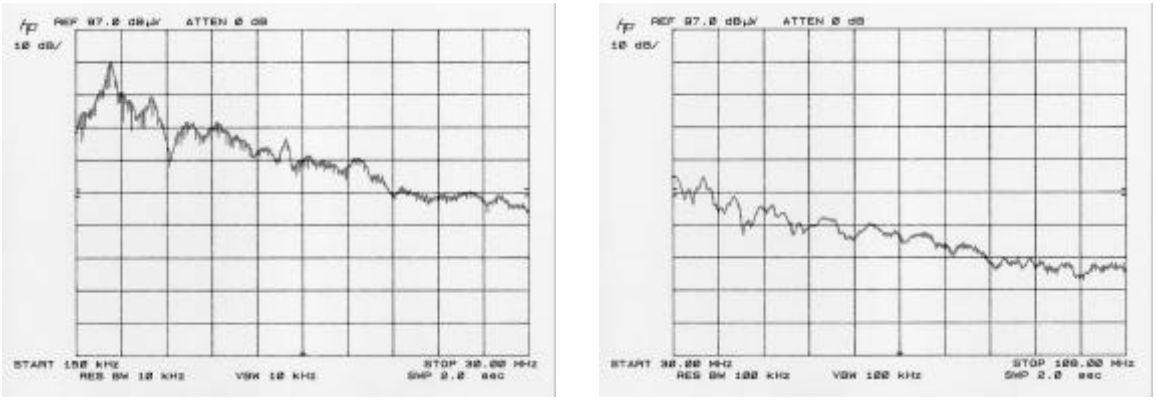

Figure 3.42 Total noise spectrum of full-bridge converter with RCD clamp.

From the noise spectrum results above, it can be found that the total noise level is higher at a frequency of 2.6 MHz, 7 MHz, 12 MHz, and 18 to 30 MHz when active clamp switch S_c is involved to realize soft-switching of S_6, S_8. In high frequency range form 30 MHz to 108 MHz, active clamp circuit increases noise level more than 20 dB.

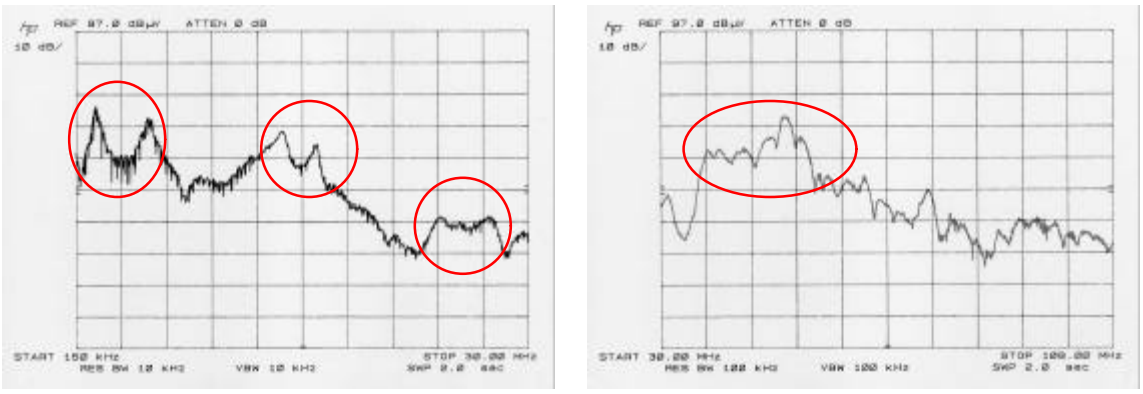

Figure 3.43 DM noise spectrum of full-bridge converter with active clamp

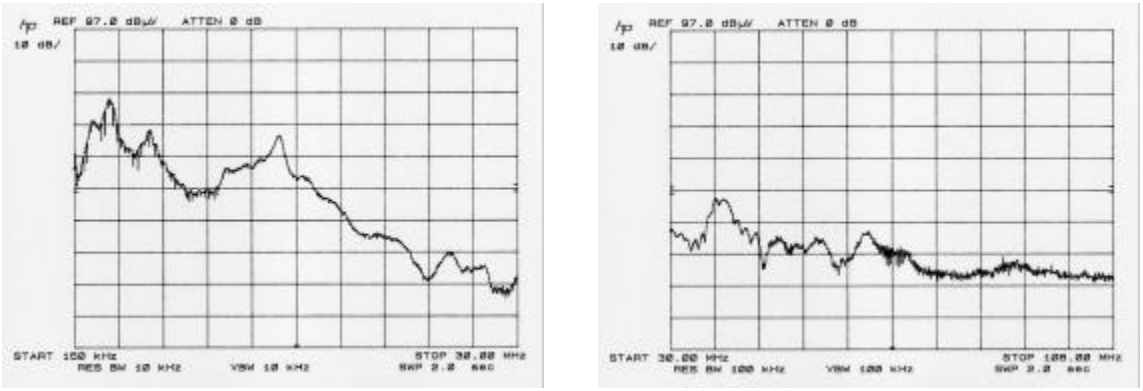

Figure 3.44 DM noise spectrum of full-bridge converter with RCD clamp

The DM noise spectrum compare shows that the active clamp circuit can increase the DM noise level by more than 10 dB at frequency 1.5, 16 and 24-27 MHz. In the high frequency range from 40 MHz to 56MHz, it increases DM noise level more than 20 dB.

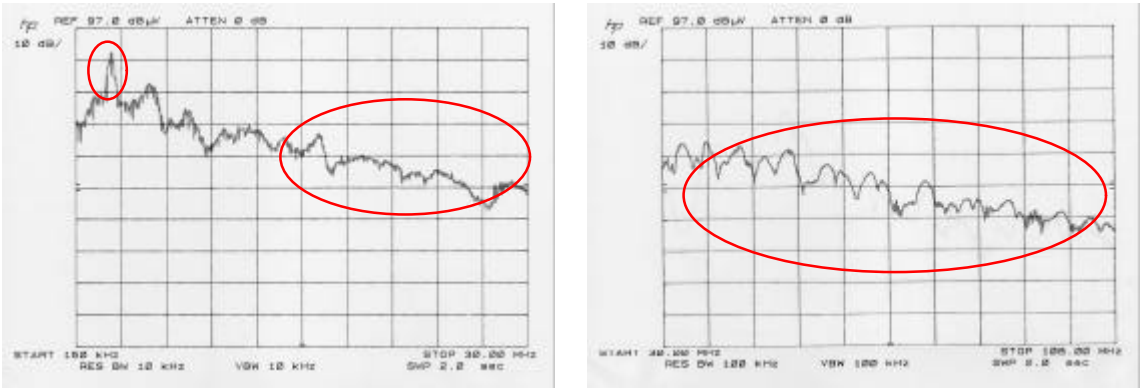

Figure 3.45 CM noise spectrum of full-bridge converter with active clamp

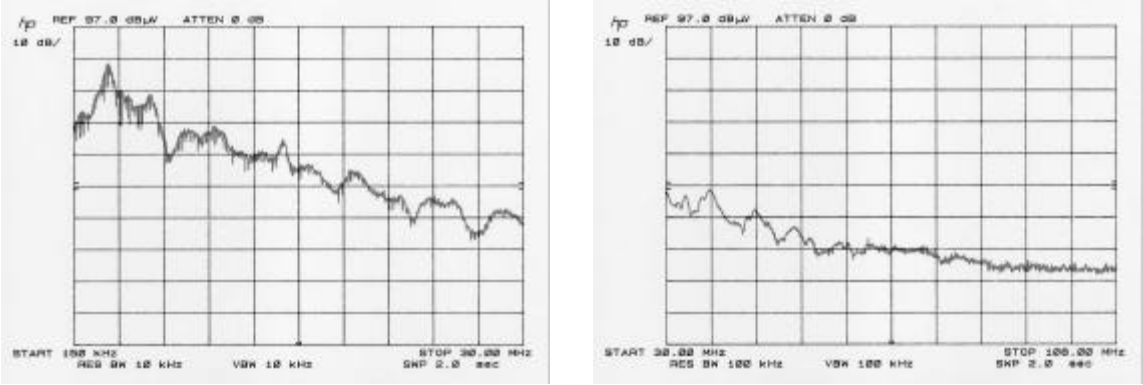

Figure 3.46 CM noise spectrum of full-bridge converter with RCD clamp

From the CM noise spectrum above, it can be found that the CM noise level is higher at frequency 2.6 MHz, and 15 to 30 MHz when active clamp circuit is involved to realize soft-switching. In high frequency range form 30 MHz to 108 MHz, the active clamp circuit increases noise level by more than 10 dB.

The final conclusion is that active clamp circuit and soft-switching in the full-bridge converter can not help to reduce the EMI noise level. On the contrary, it will cause EMI problem, especially in the high frequency range. That is because of that active clamp switch S_c is working at double frequency and hard turn-off condition. It always turns off a high current pulse. Severe voltage ringing can be found in the switch voltage waveform. In one word, active clamp switch induces EMI noise when it involves to help realize soft-switching for S_6 and S_8. The noise generated by switch S_c compensates the benefits from soft-switching.

The voltage wave form V_{CE} on auxiliary switch S_c is shown in Figure 3.47.

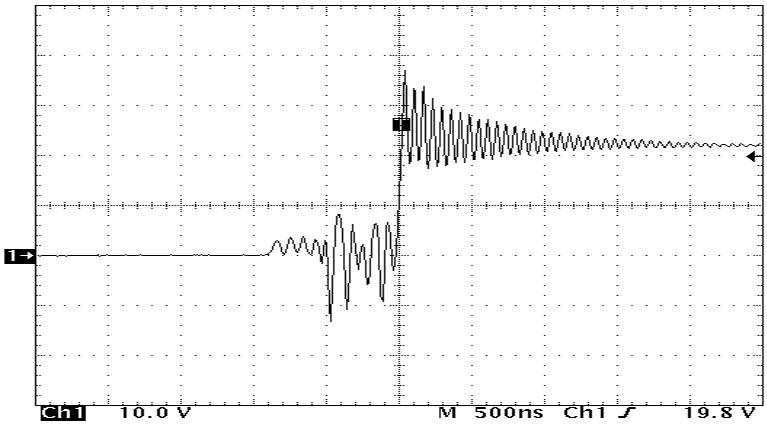

Figure 3.47 Voltage waveform on active clamp switch S_c

3.5.3 Gate resistor

It is believed the high di/dt generates differential mode noise while high dv/dt generates common mode noise. Slowing down the switching speed can help to reduce the the di/dt and dv/dt, which results in a reduced EMI noise level in spectrum. The di/dt and dv/dt can be reduced by soft-switching technology or by increasing the gate resistor.

In the full-bridge converter, complicated control timing and dead time need to be perfectly tuned because of the involvement of active clamp and synchronous rectification. Slowing down the MOSFET will be harmful to boost mode operation. Slowing down the switching speed of IGBT is a possible selection.[20]

Next, IGBT gate resisters are changed from 4.7 Ω to 15 Ω. The total noise spectrum of both case are shown in the Figure 3.48 and Figure 3.49.

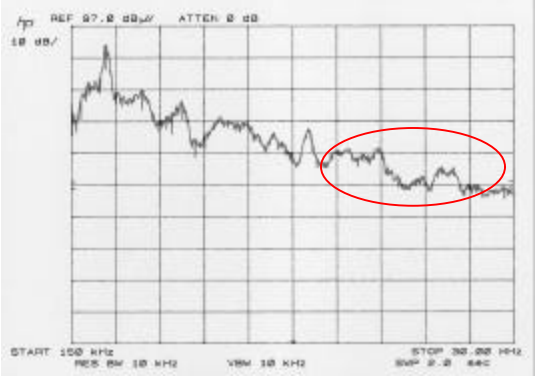

Figure 3.48 Total noise spectrum when Rg=15Ω

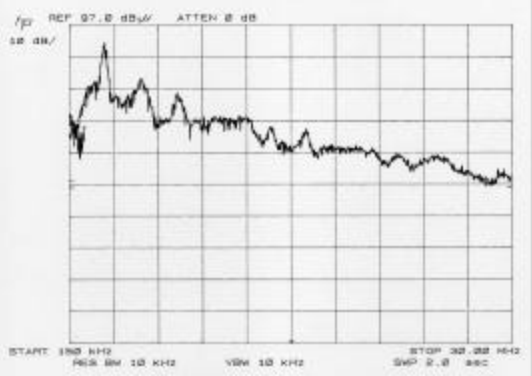

Figure 3.49 Total noise spectrum when Rg=4.7Ω

From the spectrum above, the noise level is lower as the gate resistors increase from 4.7Ω to 15 Ω. The difference is obvious in the high frequency range (10 MHz to 30 MHz). There is almost no difference in the frequency less than 10 MHz. One reason is that the IGBT in full-bridge converter is working under ZVZCS condition. The ZVS turn-on of leading leg and ZCS turn-off of lagging leg make the effect of slowing down driver speed less effective.

3.6 EMI Suppression

EMI design is called black magic because there has not been a well-defined EMI design method available. There are some techniques exist that improve the levels of EMI. In this section, EMI solutions for the two prototypes are described. EMI filter design for full-bridge converter is given. The final measurement after the EMI filter applied is given.

3.6.1 Circuit layout

The parasitic in power supply circuit play and important role in conductive EMI. For example, the capacitance between the power device and the earth or the chassis is a noise current path, a smaller capacitance means large impedance in the conductive EMI path, which result in lower EMI noise level. In the full-bridge circuit, multi-MOSFET are connected in parallel to be used as one switch. So a relatively large capacitance will exist between switch and heat sink Placing shielding between power device and heat sink will reduce this capacitance. With consideration of thermal issue, this solution is limited in this design. High current (as high as 300 A) and high di/dt exist in the converter low voltage side, which make the stray inductance in the low voltage side become important to conductive EMI. Reducing the stray inductance will help to reduce noise level in most cases.

Especially in the full-bridge circuit, current through the clamp capacitor is highly pulsating, so a low ESR capacitor with high resonant frequency is needed. The stray inductance in the low voltage side, especially the stray inductance in the active clamp branch, will generate high noise level. With the consideration above, a laminated bus

board is designed to hold the low voltage side MOSFET bridge and active clamp branch. A laminated bus can provide the lowest possible effective inductance for a circuit.[21]

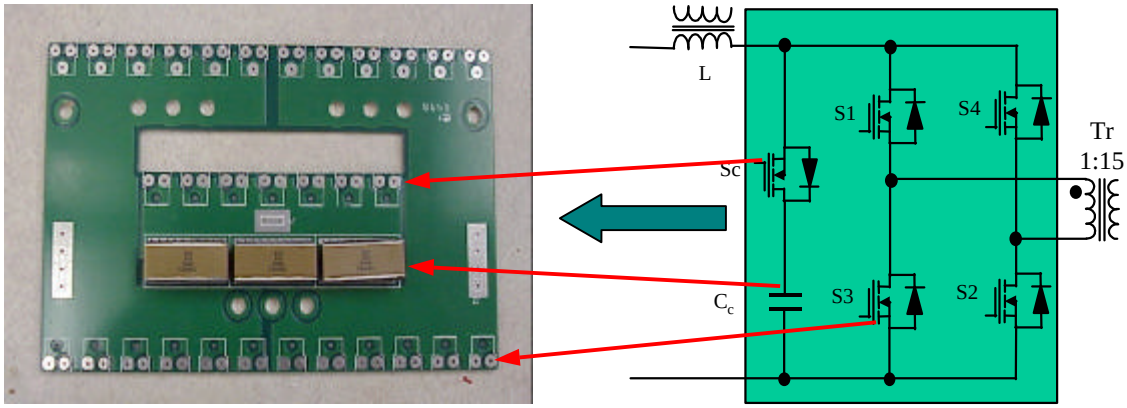

Figure 3.50 Laminated power bus board for full-bridge converter

3.6.2 Modulation of switching frequency

When the switching frequency is in the EMI test band (higher than 150 kHz), frequency modulation is a very effective way to spread the spectral energy of conductive EMI. In this way, the total EMI is unchanged, but it is possible to stay below the limits.

In this case, the switching frequency for both L-type and full-bridge converter are only 20 kHz with the consideration of power level and power loss. Frequency modulation is tested on the L-type converter and spectrum measurements show no improvement when frequency modulation technology is used.

3.6.3 EMI filter design

In this section, EMI filters are design for both L-type and full-bridge converter. A EMI filter is fabricated for full-bridge converter and final test results are shown.

3.6.3.1 EMI filter design for L-type converter

For the L-type converter when the start-up winding is disconnected, CM noise base line is shown in Figure 3.25 and DM noise base line is shown in Figure 3.27. The CM noise attenuation requiremennt is 12 dB at 530 kHz, while the DM noise attenuation is 12 dB at 1.8 MHz. From the attenuation requirements, the corner frequency can be gotten as,

$$f_{R,CM}=265 \text{ kHz}$$

$$f_{R,DM}=902 \text{ kHz}$$

If the CM capacitor C_y is chosen to be 33000 pF, and DM capacitor C_x is chosen to be 5 μF, the common mode inductor is

$$L_{CM}=5.5 \text{ μH}$$

and the differential mode inductor is

$$L_{DM}=9 \text{ nH}$$

For the L-type converter when start-up winding is connected, much higher noise level can be seen at low frequency range. CM noise base line is shown in Figure 3.24 and DM noise base line is shown in Figure 3.26. The CM noise attenuation requirement is 28 dB at 150 kHz, while the DM noise attenuation is 14 dB at 1.8 MHz. From the attenuation requirements, the corner frequency can be gotten as,

$$f_{R,CM}=30 \text{ kHz}$$

$$f_{R,DM}=902 \text{ kHz}$$

As before, if CM capacitor C_y equals 33000 pF, and DM capacitor C_x=5 μF, the common mode inductor is

$$L_{CM}=429 \text{ μH}$$

and differential mode inductor can be gotten as:

L_{DM}=9 nH

The filter design above is based on theory, it needs to be tested and corrected. But it reflects the right direction. A much bigger inductor is needed if the start-up winding is connected because start-up winding generates most of the low frequency noise (around 150 kHz). The low frequency introduced by start-up winding is CM noise. Start-up winding shows little effect on DM noise.

In the L-type circuit, common mode noise is the major noise source. To reduce the noise level, multi solution, like synchronous rectification, circuit layout, and EMI filter, are needed. While disconnect the start-up winding is the most effective way to reduce low frequency range noise level. It also reduces the common mode choke size and value dramatically.

3.6.3.2 EMI filter design for full-bridge converter

For the full-bridge converter when the start-up winding is disconnected, DM noise base line is shown in Figure 3.37 and CM noise base line is shown in Figure 3.39. The CM noise attenuation requirement is 17 dB at 530 kHz, while the DM noise attenuation requirement is 17 dB at 1.5 MHz, finally get the corner frequency:

$f_{R,CM}$=200 kHz

$f_{R,DM}$=210 kHz

If CM capacitor C_y = 33000 pF, and DM capacitor C_x = 5 μF, the common mode inductor is

$$L_{cm} = \left[\frac{1}{2*p*f_{R,cm}}\right]*\frac{1}{2*C_y} = 17mH$$

differential mode inductor is

$$L_{dm} = \left[\frac{1}{2*p*f_{R,dm}}\right] * \frac{1}{C_x} = 0.1mH$$

Figure 3.37 show the DM noise spectrum of full-bridge converter when the start-up winding is disconnected. Figure 3.38 show the DM noise spectrum when the start-up winding is connected. The low frequency range noise spectrums are almost the same. The DM noise attenuation requirements for both cases are same, 17 dB at 1.5 MHz. The DM inductor stay unchanged no matter if the start-up winding is connected or not.

The CM noise base lines are shown in Figure 3.39 and Figure 3.40. If the start-up winding is disconnected, the CM noise attenuation requirement is 17 dB at 530 kHz, and the corner frequency is 200 kHz. If start-up winding is connected, the CM noise attenuation requirement is 22 dB at 530 kHz, and the corner frequency is 120 kHz. If the start-up winding are connected, the common mode choke needs to be 26 μH to provide enough common mode noise attenuation.

The EMI filter design result can be summarized as follow:

EMI filter design		L_{CM}	L_{DM}
L-type converter (C_x=5 μF, C_Y=33000pF)	Start-up winding Connected	429 μH	9 nH
	Start-up winding Disconnected	5.5 μH	9 nH
Full-bridge converter (C_x=5 μF, C_Y=33000pF)	Start-up winding Connected	26 μH	0.1 μH
	Start-up winding disconnected	17 μH	0.1 μH

3.6.4 Final EMI spectrum measurement

This bi-directional DC/DC converter has active switches on both sides of an isolation transformer. What is the most concerned is the noise level on the low voltage side in buck

mode. In the buck mode operation, all switches on both sides are active. Noise source can be switches from both sides. For this reason, another EMI filter is connected to the high voltage side as shown in the Figure 3.51.

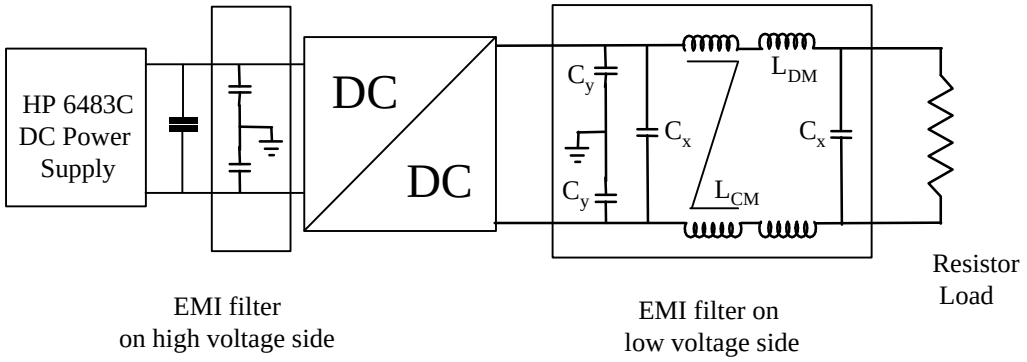

Figure 3.51 Schematic of EMI filter system

Generally speaking, localizing EMI noise is another effective solution to reduce EMI noise level. The high side filter here is only a pair of common mode capacitors which are arbitrarily selected as 0.1 μF.

Base on the theory calculation above, one EMI filter for full-bridge converter is built and tested. The final test result is shown in Figure 3.54.This result is based on multi EMI solution that includes opening start-up winding, filters on both sides.

In the final test, in order to pass Ford's EMI standard, the designed filter parameters are corrected. The common mode choke is increased to 19 μH and the differential mode inductor is increased to 1 μH. Both of them are implemented with high permeability torrid core. The capacitors are kept as the theory design, Cx=5 X 1 μF and C_y=10 X 3300 pF. In theory, large capacitor means small inductor value, but a large capacitor will have lower resonant frequency, which will make the filter worse. So, capacitors are selected relatively small and several small capacitors connected in parallel get better performance.

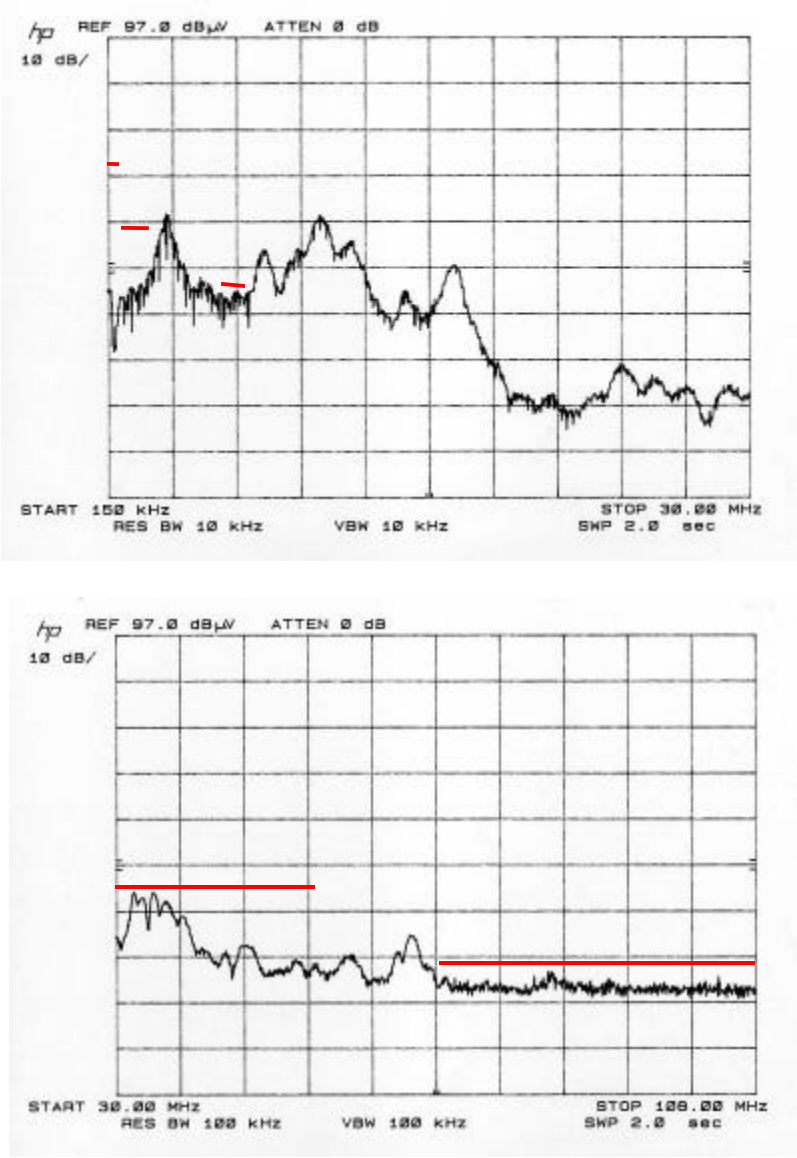

Figure 3.52 Total EMI noise spectrum after EMI filter

(Ford EMI standard is labeled in the photo)

From Figure 3.52 above, it can be seen that the full-bridge converter can pass the EMI requirement with the designed EMI filter. The detailed performance of the EMI filter can be gotten from the CM noise spectrum in Figure 3.54 and the DM noise spectrum in Figure 3.53.

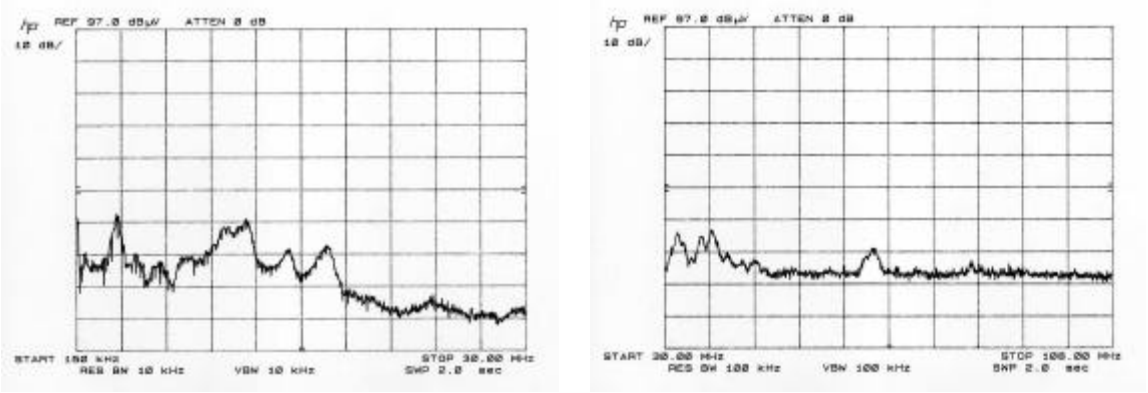

Figure 3.53 DM noise spectrum after EMI filter

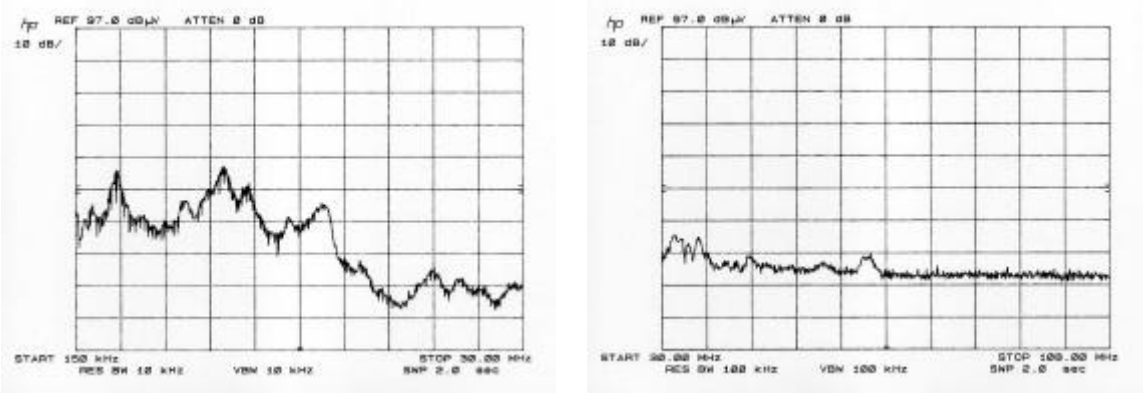

Figure 3.54 CM noise spectrum after EMI filter

3.6.5 Conclusion

In both L-type and full-bridge converter, CM noise makes the major contribution to the total noise. Several solutions are used to reduce the EMI noise level, which includes opening start-up winding to eliminate an EMI source, using synchronous rectifier to improve diode reverse recovery, and localizing EMI noise by add an EMI filter on both side of isolation transformer. Satisfied results are gotten after all these solutions are applied.

CHAPTER IV
CONCLUSIONS AND FUTURE WORK

In this chapter, conclusions from the research efforts are described. Future research work is also suggested.

4.1 Conclusions

- EMI noise problem in a vehicular bi-directional converter is complicated because of bi-directional capability. Normally, only noise level on the low voltage side is regulated
- Two bi-directional DC/DC converters have been built and tested. Multi EMI solutions were investigated. Their effects were shown by noise spectrum measurements.
- In both prototypes, total noise is mainly contributed by CM noise, which is much higher than DM noise. Reducing CM noise is an effective way to reduce the total noise.
- In L-type converter, the synchronous rectification technology used can help to improve the diode reverse recovery problem by shift current from the diode to MOSFET before diode turn-off. Improved diode reverse recovery leads to lower DM noise in certain frequency range. This improved DM noise level is also shown to help the total noise spectrum.
- In full-bridge converter, soft switching is realized by the operation of active clamp branch. The active clamp switch is working under hard switching condition and at double switching frequency. The noise introduced by active clamp switch offsets the

improvement from soft-switching. In total noise spectrum, no big improvement is gotten by soft switching.

- The auxiliary start-up winding in both L-type converter and full-bridge converter is proven to be both a noise source and a noise path. Its effect on the EMI spectrum concentrates in the low frequency range. The auxiliary Start-up winding affects CM noise more than DM noise. Opening the start-up winding loop with a mechanical switch can help to reduce the noise level and EMI filter size. EMI filter for the full-bridge converter is designed and tested. Final EMI spectrum measurements show that the filter designed can satisfy the EMI specification.
- A new concept, putting EMI filter on both sides of bi-directional converter is proposed.
- Multi EMI solutions are used together to get best EMI results.

4.2 Future work

In a fuel cell vehicle, a traction inverter and traction motor will be connected to the fuel cell output bus, which also connect to the high voltage side of the bi-directional DC/DC converter. Due to the power level of the traction system, a high noise level is expected on the high voltage bus. Especially high CM noise level is expected because of the relatively big coupling capacitance between electric motor and ground (chassis in vehicle). Under this situation, the bi-directional DC/DC converter will be a critical noise path, which connects the low voltage bus and high voltage bus. The noise emission from high voltage bus will go through this converter to the low voltage system.

The research work done in this paper is about suppressing the noise generated by the converter. More research works on EMI noise in the overall system and the EMI noise propagation through this converter should continue.

REFERENCE

[1] "Gordon Research Conference on Fuel Cells", Plymouth State Collage, June, 1999.

[2] K. Wang, J. Zhang, C.Y. Lin, W. Chen, W.G. Odendaal, D. Qu, J. Lai, F.C. Lee, "An Isolated Bi-Directional DC-DC Converter with High Conversion Ratio" Phase I. July, 1997.

[3] Ford Motor Company, "Ford CE420 Conductive EMI Specification"

[4] Yuqing Tang, "High Power Inverter EMI Characterization and Improvement Using Auxiliary Resonant Snubber Inverter". Master Thesis CPES 1998

[5] Donbing Zhang, Dan Y. Chen, Fred C. Lee, "An Experimental Comparison of Conducted EMI Emissions between a Zero-Voltage Transition Circuit and a Hard Switching Circuit", PESC96, page 1992-1997.

[6] Qing Chen, "Electromagnetic Interference (EMI) Design Consideration for a High Power AC/DC Converter", PESC98, page 1159-1164.

[7] Ting Guo, "Seperation of the Common-mode and the Differential- mode onducted electromagnetic Interference Noise" Master's thesis 1994 VPEC.

[8] J.A.Ferreira, P.R.willcock, S.R. Holm, "Sources, Paths and Traps of Conducted EMI in Switch Mode Circuits", IAS 97, page 1584-1591.

[9] K. Wang, F.C. Lee, and J. Lai, "Bi-directional full-bridge DC/DC converter with unified soft-switching scheme, part I: principle of operation," Proceeding of VPEC Seminar, 1998, pp. 143-150.

K. Wang, L. Zhu, D. Qu, H. Odendaal, J. Lai, and F.C. Lee, "Bi-directional full-bridge DC/DC converter with unified soft-switching scheme, part II: design,

implementation, and experimental results," Proceeding of VPEC Seminar, 1998, pp. 150-156.

[10] Alberto Guerra, Franco Maddaleno, Marco Soldano, " Effects, of Diode Recovery Characteristics on Electronmagnetic Noise in PFCs. APEC 98.

[11] Alberto Guerra, Franco Maddaleno, "Effects of Diode Recovery Characteristics on Electromagnetic Noise in PFCs", APEC98.

[12] P.R. Willcock, J.A. Ferreira, J.D. Van Wyk, "An Experimental Approach to Investigate the Generation and Propagation of Conducted EMI in Converters", PESC98, page 1140-1145.

[13] Nobuhiko Yamashita, Naoki Murakami, Toshiaki Yachi, "Conduction Power Loss in MOSFET Synchronous Rectifier with Parallel-Connected Schottky Barrier Diode", IEEE Transactions on Power Electronics, vol. 13, NO. 4, July 1998.

[14] Laszlo Balogh, "The Current-Doubler Rectifier: An Alternative Rectification Technique for Push-Pull and Bridge Converters", Unitrode Design Note, DN63.

[15] Peter J. Wolfs, "A Current-Sourced DC-DC Converter Derived via the Duality Principle from the Half-Bridge Converter", IEEE Transactions on Industrial Electronics, vol. 40, NO.1, February 1993.

[16] Nasser H. Kutkut, Glen Luckjiff, "Current Mode Control of a Full Bridge DC/DC Converter with a Two Inductor Rectifier", PESC97.

[17] Brian Acker, Charles R. Sullivan, "Synchronous Rectification with Adaptive Timing Control", PESC95, page 88-95.

[18] S.R. Holm, J.A. Ferreira and P.R. Willcock, “Soft Switching Technique for Lowering Conducted EMI on a three Phase Boost Converter”, PESC98.

[19] F. Caricchi, F. Giulii Capponi, L. Solero, “Study of Bi-directional Buck-Boost Converter Topologies for Application in Electrical Vehicle Motor Drives”, PESC98, page 287-293.

[20] I. Zverev, S. Konrad, H. Voelker, “ Influence of the Gate Drive Techniques on the Conducted EMI Behavior of a Power Converter”, PESC 97.

[21] James M. Allocco, “Laminated Bus Bar for Power System Interconnects”, PESC97 page 585-589.

[22] K. Wang, C. Y. Lin, L. Zhu, D. Qu, F. C. Lee, J. Lai, “Bi-directional DC to DC converters for fuel cell systems,” Proceeding of IEEE APEC 1998, pp. 47-51.

VITA

Dayu Qu, was born in Shandong province, China, on July 4th, 1970. He received his B.S. degree in Department of Industry Automation in 1992 and M.S. degree in 1995, both from Tianjin University. Since 1997, he has been a MS. student in Electric Engineering Department in Virginia Polytechnic Institute and State University, Blacksburg, Virginia.

From 1992 to 1997, he was a research assistant in Chinese National Combustion Engine Laboratory, Tianjin University, China. In 1997, He joined Virginia Power Electronics Center as a research assistant and studied toward a MS. degree in power electronics area. His interests are high frequency power electronic conversion, EMI reduction technology, and control of power electronics system.

Dayu Qu